

May 2014

Investigation of TiO₂ and InVO₄-TiO₂ Semiconductors for the Photocatalytic Degradation of Aqueous Organics

Sandra L. Pettit

University of South Florida, eng.pettit@gmail.com

Follow this and additional works at: <http://scholarcommons.usf.edu/etd>

 Part of the [Chemical Engineering Commons](#)

Scholar Commons Citation

Pettit, Sandra L., "Investigation of TiO₂ and InVO₄-TiO₂ Semiconductors for the Photocatalytic Degradation of Aqueous Organics" (2014). *Graduate Theses and Dissertations*.
<http://scholarcommons.usf.edu/etd/5103>

This Dissertation is brought to you for free and open access by the Graduate School at Scholar Commons. It has been accepted for inclusion in Graduate Theses and Dissertations by an authorized administrator of Scholar Commons. For more information, please contact scholarcommons@usf.edu.

Investigation of TiO₂ and InVO₄-TiO₂ Semiconductors for the Photocatalytic Degradation of
Aqueous Organics

by

Sandra L. Pettit

A dissertation submitted in partial fulfillment
of the requirements for the degree of
Doctor of Philosophy in Chemical Engineering
Department of Chemical and Biomedical Engineering
College of Engineering
University of South Florida

Major Professor: John N. Kuhn, Ph.D.
Norma A. Alcantar, Ph.D.
Jeffrey A. Cunningham, Ph.D.
David P. Fries, M.S.
Babu Joseph, Ph.D.

Date of Approval:
March 17, 2014

Keywords: titania, geosmin, MIB, aquaculture, photocatalysis

Copyright © 2014, Sandra L. Pettit

ACKNOWLEDGMENTS

Dr. John T. Wolan provided the inspiration to start graduate studies and the support to begin research endeavors. *Dr. John N. Kuhn* offered support and reassurance during a difficult transition, encouraged me to join his research group, and afforded just the right amount of guidance and freedom. Graduate committee members provided valuable insight to technical writing, data analysis, and equipment operation. Thank you to *Dr. Norma Alcantar*, *Dr. Jeffrey Cunningham*, *Dr. Babu Joseph*, and *Mr. David Fries*.

Mr. Robert Tufts and his team from the *Nanotechnology Research and Education Center* provided extensive training for X-ray diffraction, scanning electron microscopy, and energy dispersive X-ray spectroscopy. *Dr. Yangyang Zhang* and *Mr. Chuck Garretson* from the *Clean Energy Research Center* were instrumental in building and maintaining photoreactors.

Ms. Cheryl McCane, my undergraduate colleague, continually questioned and inspired. During long hours in the lab and conference travel, we learned much from each other. And finally, I would like to acknowledge my lab and project partners: *Lyndsey Baldyga Figler*, *Geran Barton*, *Yolanda Daza*, *Brian Gregson*, *Gary Hendrick*, *Selma Hokenek*, *Jorge Lara Viera*, *Bijith Mankidy*, *Louis Rufo*, *Bradley Ridder*, *Timothy Roberge*, *Laura Rodriguez-Gonzalez*, *Phil Saraneeyavongse*, and *Devin Walker*. They provided encouragement, inspiration, and commiseration.

TABLE OF CONTENTS

LIST OF TABLES	iii
LIST OF FIGURES	iv
ABSTRACT	vii
CHAPTER 1: INTRODUCTION AND BACKGROUND	1
1.1 Introduction	1
1.2 Photocatalysis	3
1.2.1 Electrical Properties	3
1.2.2 Titanium Dioxide	5
1.3 Aqueous Organic Pollutants	7
1.3.1 Methyl Orange	7
1.3.2 Geosmin and MIB	8
1.4 Aquaculture	9
CHAPTER 2: EXPERIMENTAL METHODOLOGY	16
2.1 Syntheses	16
2.1.1 Synthesis of InVO ₄	16
2.1.2 Synthesis of InVO ₄ -TiO ₂ Composites	20
2.2 Characterization	20
2.2.1 Fourier Transform Infrared Spectroscopy	20
2.2.2 X-ray Diffraction	21
2.2.3 Scanning Electron Microscopy and Energy Dispersive X-ray Spectroscopy	21
2.3 Quantification and Measurement	21
2.3.1 Methyl Orange	21
2.3.2 Geosmin and MIB	23
2.4 Photoreactor	26
2.4.1 Batch Slurry Reactor	26
2.4.2 Flow Reactor	28
CHAPTER 3: PURE AND MIXED PHASE TITANIA COMPOSITES	30
3.1 Introduction	30
3.2 Experimental	33
3.2.1 Chemicals	33
3.2.2 Synthesis of InVO ₄	33
3.2.3 Preparation of InVO ₄ -TiO ₂ Composites	33

3.2.4 Characterization	34
3.2.5 Photocatalytic Activity.....	34
3.3 Results and Discussion	35
3.4 Conclusions.....	39
CHAPTER 4: PHOTOCATALYTIC DEGRADATION OF GEOSMIN AND MIB.....	41
4.1 Introduction.....	41
4.2 Experimental.....	44
4.2.1 Chemicals and Materials.....	44
4.2.2 Analytical Method for Geosmin and MIB Quantification.....	44
4.2.3 Experimental Reactor System.....	45
4.3 Results and Discussion	46
4.4 Conclusions.....	52
CHAPTER 5: APPLIED PHOTOCATALYSIS AT MOTE MAP	53
5.1 System Set-up and Placement.....	53
5.2 Results and Discussion	55
CHAPTER 6: CONCLUSIONS AND FUTURE WORK.....	59
6.1 Conclusions.....	59
6.2 Future Work.....	60
6.2.1 Pure and Mixed Phase Titania	60
6.2.2 Visible Light Photoinitiation for MIB and Geosmin Reduction.....	60
REFERENCES	62
APPENDICES	68
Appendix A Copyright Permissions	69
A.1 Permission for Use of Material in Figure 1.....	69
A.2 Permission for Use of Material in Figure 2.....	70
A.3 Permission for Use of Material in Chapter 3	71
Appendix B Instrumentation.....	72
Appendix C Supplemental Data.....	75

LIST OF TABLES

Table 1 Geosmin and MIB Detection Limits.....	26
Table 2 Ions (m/z) Monitored in SIM Mode GC-MS for Analyte Quantification	45
Table 3 Pseudo-first Order Rate Constants (k_{app}) and System Initial pH and Dissolved Oxygen (DO) Content.....	50
Table 4 Water Analysis.....	54
Table 5 MIB and Geosmin Reduction	57

LIST OF FIGURES

Figure 1 Photon Absorption and Charge Transport Pathways.....	5
Figure 2 TiO ₂ Crystalline Structures.....	6
Figure 3 Molecular Structure of Methyl Orange	8
Figure 4 Molecular Structures of (a) Geosmin and (b) MIB	9
Figure 5 Schematic of Water Treatment at MOTE MAP	10
Figure 6 Fish Culture Tanks	11
Figure 7 Drum Filter	11
Figure 8 Nitrification System.....	12
Figure 9 Anaerobic Denitrification Reactor	12
Figure 10 Degassing Weir	13
Figure 11 Oxygenation Compartment	14
Figure 12 Purge Tank.....	15
Figure 13 Molecular Structure of DTPA	17
Figure 14 FTIR Spectrum of Indium-Vanadium-DTPA Complex.....	17
Figure 15 FTIR Spectrum of InVO ₄ Powder (Post Calcination).....	18
Figure 16 XRD Stick Patterns of Synthesized and Orthorhombic Reference InVO ₄	19
Figure 17 SEM Images of InVO ₄ at 5k and 10k Magnification	19
Figure 18 EDS Spectrum of Synthesized InVO ₄	20
Figure 19 Centrifuged Methyl Orange Aliquots.....	22

Figure 20 UV-Vis Absorbance of Methyl Orange.....	22
Figure 21 SPME Assembly.....	24
Figure 22 Calibration Curves for Quantification of Geosmin and MIB.....	25
Figure 23 Batch Slurry Reactor	27
Figure 24 Photoreactor Enclosure.....	27
Figure 25 Flow Reactor with Removed Cover	29
Figure 26 Flow Reactor System.....	29
Figure 27 XRD Patterns of Synthesized InVO ₄ , Pure and Mixed Phase TiO ₂ , and InVO ₄ - TiO ₂ Composites.....	35
Figure 28 SEM Image of Synthesized InVO ₄	36
Figure 29 Secondary Electron Microscopy (SEM) Image of 5% InVO ₄ -TiO ₂ (P-25) with Elemental Mapping (EDS) of Ti K in Green and In L in Red.....	37
Figure 30 EDS Spectrum of 5% InVO ₄ -TiO ₂ (P-25).....	37
Figure 31 SEM Micrograph of 5% InVO ₄ -TiO ₂ (P-25).....	38
Figure 32 Photocatalytic Degradation of Methyl Orange.....	39
Figure 33 SIM Mode GC Chromatogram Displaying IBMP and MIB with Inset Figure of MIB Mass Spectrum	47
Figure 34 SIM Mode GC Chromatogram Displaying Geosmin with Mass Spectrum Inset Figure.....	47
Figure 35 Geosmin Degradation Based on Normalized Concentrations	49
Figure 36 Determination of Pseudo-first Order Rate Constants for Geosmin Degradation.....	49
Figure 37 Placement of Bench Scale Reactor at MOTE MAP	54
Figure 38 MOTE MAP Bench Scale Reactor System	55
Figure 39 SIM Mode GC Chromatogram Displaying IBMP and MIB with Inset Figure of MIB Mass Spectrum	56

Figure 40 SIM Mode GC Chromatogram Displaying Geosmin with Mass Spectrum Inset Figure.....	56
Figure 41 Comparison of UV Initiated TiO ₂ and Visible Light Initiated TiO ₂ -InVO ₄ Composite for the Photocatalytic Degradation of Geosmin and MIB.....	61
Figure B-1 Bio Rad Excalibur FTS 3000 FTIR – External and Internal Views.....	72
Figure B-2 PIKE ATR Sample Holder	72
Figure B-3 Perkin Elmer Lambda 35 UV-Vis Spectrometer (a) with Dual Beam Detection (b).....	73
Figure B-4 Eppendorf Centrifuge	74
Figure B-5 Perkin Elmer Clarus GC-MS.....	74
Figure C-1 5% InVO ₄ -TiO ₂ SEM Images and EDS Elemental Maps with Progressive Magnification.....	75
Figure C-2 Typical Time Lapsed Methyl Orange Absorbance	76
Figure C-3 Effect of Catalyst Dosing Rate on Methyl Orange Degradation.....	76
Figure C-4 Effect of Mixing Rate on Methyl Orange Degradation.....	77
Figure C-5 Effect of InVO ₄ Dopant Concentration on Methyl Orange Degradation.....	77

ABSTRACT

Water is a vital natural resource. To develop more sustainable water systems, we must focus efforts on the removal of persistent contaminants. Aqueous organic contaminants include azo dyes, halogenated organics (e.g. pesticides), and algal and bacterial metabolites. The latter are common to surface waters and freshwater aquaculture systems and can cause taste and odor problems. Two of the principal organoleptic compounds are geosmin and 2-methylisoborneol (MIB). Traditional oxidation treatment methods, utilizing chlorine, hydrogen peroxide, and potassium permanganate, have been employed with varying levels of efficacy for removal of these and other organic contaminants. Advanced Oxidation Processes (AOPs) have greater potential for the removal of persistent contaminants than traditional methods due to their higher pollutant removal rates, their ability to degrade a variety of organic material, and their ability to completely mineralize compounds [1].

An emerging AOP technology is the use of titania based photocatalysts for water treatment. Titanium dioxide (TiO_2) is an effective, inexpensive, and stable photocatalyst used for the decomposition of aqueous organics. Titania is primarily activated by the ultraviolet portion of the spectrum due to its energy band gap of 3.0-3.2 eV (depending upon crystalline structure). Photocatalytic efficiency can be enhanced or tuned through the use of semiconductor dopants and the variance of titania crystal structure (i.e. anatase to rutile ratios). Metal oxides, like indium vanadate (InVO_4), may enhance reaction rates through new interfacial reaction sites and electron scavenging, transport, and storage. InVO_4 has been shown to have four sub-

bandgap transitions, of which three are in the visible range [2]. In this work, the synthesis of InVO₄-TiO₂ composite semiconductors is examined to shift photo-initiation into the visible portion of the spectrum. Parametric studies of the visible spectrum photodegradation of methyl orange, an azo dye, and 2-chlorophenol provide a basis for analysis. Methyl orange was utilized to ascertain the effect of pure and mixed phase titania in the semiconductor composites.

The TiO₂ photodegradation of geosmin and MIB has been previously demonstrated in small-scale batch slurry reactions. Slurry systems require the downstream separation of catalyst from the liquid. Laboratory trials use centrifugation or micro-filtration. Alternatively, immobilization of the photocatalyst could allow scale-up of the process. Here, titania was immobilized on glass plate substrates using an ethanol spray technique.

Finally, naturally tainted waters may contain a number of constituents in addition to the target compounds. In recirculating aquaculture systems, the water contains natural organic matter (NOM), ammonia, nitrite/ nitrate, and carbonate species. These constituents may block light penetration, block reaction sites, scavenge hydroxyl radicals, or affect the surface chemistry of the catalyst. Further, geosmin and MIB concentrations are extremely low, in the ppt range. Naturally tainted waters from MOTE Marine Laboratory Aquaculture Research Park are treated in the laboratory and *in situ* to demonstrate TiO₂ degradation efficiency for trace concentration geosmin and MIB degradation in a complex water matrix.

CHAPTER 1: INTRODUCTION AND BACKGROUND

1.1 Introduction

Titanium dioxide (TiO₂), also known as titania, is a stable and effective photocatalyst for the degradation of organic compounds in gaseous and aqueous systems. Degradation reactions include the decomposition of acetaldehyde [3], acetone [4], chloroform [5], chlorophenols [6, 7], dyes (e.g. methyl orange and methylene blue) [8-16], insecticides (e.g. monocrotophos) [17], and many other organic compounds. Recently, TiO₂ has garnered significant attention as an emerging water treatment technology for persistent organic contaminants [1, 9, 18].

Titania crystalline phases include the photoactive polymorphs, anatase and rutile. Although individually photoactive, they generally display enhanced photocatalytic properties in mixed phase systems [15, 19-26]. Relative photoactivity of pure and mixed phase titania is dependent upon the type of reaction under investigation [3, 20]. Studies have shown that the optimal rutile content can vary between 10 to 70% depending upon the reaction of interest [20].

Due to titania's band gap of 3.0-3.2 eV, ultra violet (UV) light is used as the photo-initiation source. Many approaches have been attempted to shift photo-initiation into the visible range and to increase photoactivity through the reduction of recombination rates and improvement of charge transfer. One approach involves doping the catalyst with nonmetal ions, such as nitrogen [9, 27-29], carbon [30], and sulfur [13]. Metal ion [5, 8, 31] and metal oxide [17, 32] doping have also been investigated.

Doping can be achieved through ball milling of the catalyst with ion specific precursors [4, 14] or with metal oxides and mulling agents [17, 33]. The drawback of this approach is that

ball milling induces a phase transformation of titania crystals from anatase to rutile [33-35]. The phase transformation can lead to less than or greater than desirable rutile to anatase phase ratios. Further, ball milling may lead to crystal agglomeration and reduction of active surface area [33-35].

Other synthesis methods include acidic colloidal suspensions [5] and reflux/thermal methods [8, 9, 12, 28, 31, 32, 36]. These methods generally result in doped anatase phase catalysts [8, 28, 32, 36, 37]. Heat treatment can be utilized to phase shift a portion of the anatase crystals to rutile. However, heat treatment causes aggregation and sintering which result in a decrease of photoactivity [5, 20].

Photocatalytic initiation and efficiency can be enhanced or tuned through the use of dopants and the variance of titania crystal phase ratios. Existing synthesis methods allow the independent variance of only one parameter. Previous attempts to modify crystal phase after doping resulted in loss of photoactivity due to sintering and aggregation. Development of a novel synthesis method which allows the independent adjustment of dopant and crystal phase ratio would allow the tailoring of catalysts to meet contaminant-specific needs.

The ability to tailor the catalyst to increase the photocatalytic efficiency to degrade target compounds could lead to its use in new applications for air and water treatment. One targeted application is the removal of off-flavor compounds, 2-methylisoborneol and geosmin, from recirculating aquaculture systems. Two challenges associated with this application are the trace levels (ppt) of the contaminants and the complex water matrix. Photocatalytic degradation of organic compounds with low concentrations has been shown to generally follow pseudo-first order kinetics [6, 11, 38-41]. Since the rate is dependent on contaminant concentration, extremely low initial concentrations result in slow reaction rates. Moreover, the complex water

matrix contains natural organic matter (NOM) and carbonates, which are known hydroxyl radical scavengers that can further reduce target compound degradation [1]. Demonstration of titania's ability to decompose MIB and geosmin in natural water would advance the technology as a feasible water treatment alternative.

The *long term goal* is to develop a commercially viable visible range photocatalytic oxidizer for the decomposition of organics in aqueous systems. The *overall objective* of this work is preliminary development of a tunable photocatalyst and demonstration of photocatalysis as an effective method for the removal of off-flavors from recirculating aquaculture systems. The execution of the following *specific goals* will lead to the accomplishment of the overall objective.

1. Development of a novel synthesis method, which allows the independent variance of dopant material and titania crystal phase.
2. Elucidation of the correlation between crystalline phase and dopant effects.
3. Demonstration of the reduction of target, trace level concentration contaminants in a complex water matrix.

1.2 Photocatalysis

1.2.1 Electrical Properties

Photocatalysis starts with the initial absorption of photons by a molecule or material to produce electronically excited states. The excited states are highly reactive and quickly undergo a de-excitation event. To understand this process, the concepts of energy bands, band gap, and charge transport will be introduced.

Electrons of an individual atom may exist at a number of different energy levels. As the interatomic distance between atoms decreases, the difference in energy of electrons in a given

orbital (e.g. 1s, 2s, 2p) becomes smaller. In solid materials, the energy difference between electrons in an orbital becomes exceedingly small, and this small range of energy is called an energy band. In the ground state, electrons occupy the bands with the lowest available energy states. The highest energy, occupied band of the ground state is the valence band. When an electron is excited with sufficient energy, it can move from the valence band into a higher energy band, known as the conduction band. Electrons in the conduction band are not bound to an individual atom and can move freely through the atomic lattice.

The difference in energy between the valence and conduction bands is the band gap. Insulators have a large band gap and effectively prohibit the excitation of electrons into the conduction band. In metals, the valence and conduction bands overlap allowing electrons to move freely throughout the atomic lattice. The band gap in semiconductors is small enough to be traversed when an electron is excited but large enough to obstruct free electron conduction. For TiO₂, the band gap ranges from 3.0 to 3.2 eV, depending upon the crystalline structure. This energy range corresponds to light in the near ultraviolet (UV) to violet range, thus making TiO₂ a suitable material for photocatalysis. The width of the band gap and the band edges (i.e. the upper and lower energy limits) can be distorted by altering the physical properties of the semiconductor.

When TiO₂ is activated by light of an appropriate wavelength, photon absorption causes an electron to be excited to the conduction band leaving a vacancy in the valence band (Figure 1 inset). This is known as the creation of an electron-hole pair. The conducting band electron (e_{cb}^-) and valence band hole (h_{vb}^+) are highly reactive. Pathways for their de-excitation are shown in Figure 1.

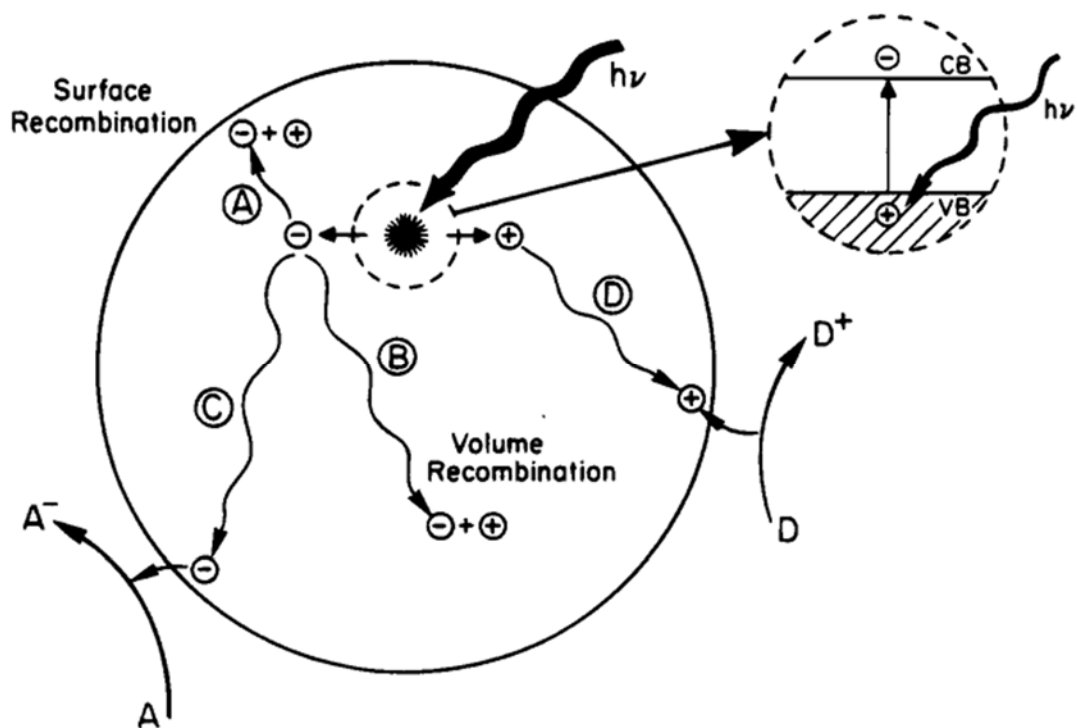


Figure 1 Photon Absorption and Charge Transport Pathways. Reprinted (adapted) with permission from Linsebigler [42]. Copyright 1995 American Chemical Society

Migration of the charge carriers to the catalyst surface (pathways C and D) is desired. At the surface, electrons reduce an electron acceptor and holes oxidize an electron donor. Surface recombination (pathway A) and volume recombination (pathway B) of the electron and hole are detrimental to photocatalytic efficiency. Recombination is generally accompanied by the release of photons, phonons, or heat. Modifications to the semiconductor, which inhibit recombination by trapping charges or increasing charge separation, increase the quantum yield of the photocatalytic process.

1.2.2 Titanium Dioxide

Titanium dioxide (TiO_2) can exist as an amorphous material or in numerous crystalline forms. Photoactive polymorphs include anatase, rutile, and brookite [20]. However, limited investigation has been reported on the use of brookite as a photocatalyst. Anatase and rutile both

have a body centered tetragonal unit cell, where the center titanium cation is surrounded by an octahedron of six oxygen atoms. They differ in their axial spacing and interstitial angles between oxygen planes. Rutile has dimensions of $a = 4.593 \text{ \AA}$ and $c = 2.959 \text{ \AA}$ and angles of 81.21° and 90° , while anatase has dimensions of $a = 3.784 \text{ \AA}$ and $c = 9.515 \text{ \AA}$ and angles of 78.12° and 92.43° [42]. The differences in the two structures are best illustrated by a comparison that includes views from the perspective of their respective common planes as shown in Figure 2.

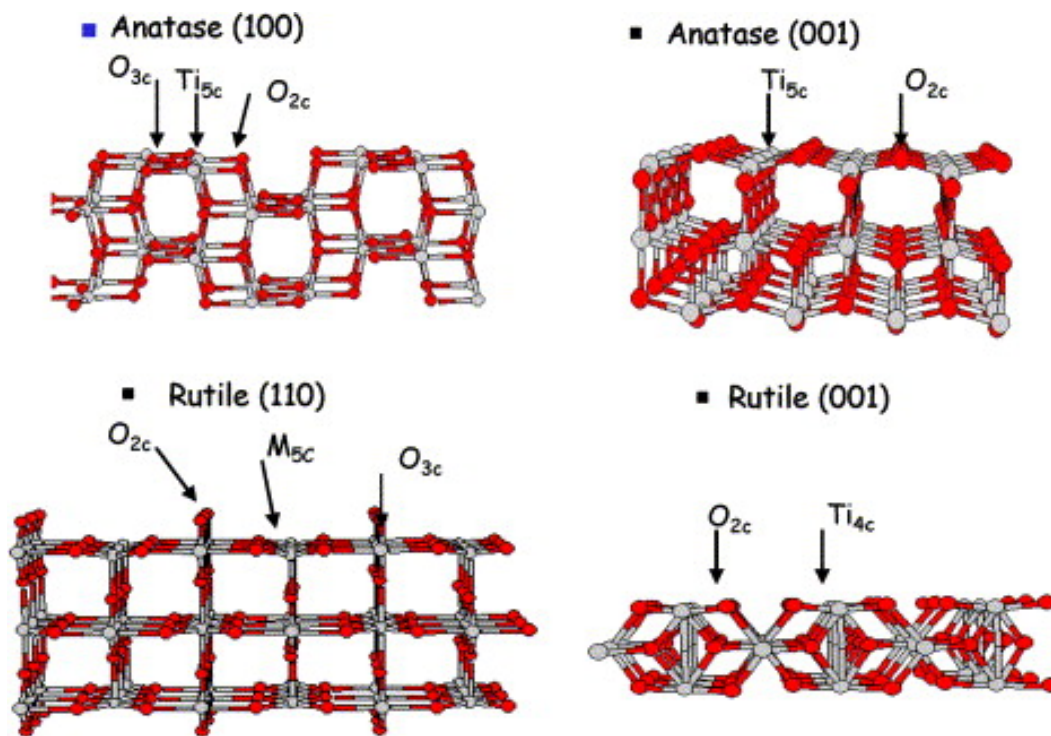


Figure 2 TiO₂ Crystalline Structures. Reprinted from Surface Science, 583/1, A. Bouzoubaa, A. Markovits, M. Calatayud, C. Minot, *Comparison of the reduction of metal oxide surfaces: TiO₂-anatase, TiO₂-rutile and SnO₂-rutile*, 110, Copyright (2005), with permission from Elsevier [43].

Anatase and rutile, although both individually photoactive, generally display enhanced photocatalytic properties in mixed phase systems [15, 19-26]. However, relative photoactivity of pure and mixed phase titania is dependent upon the type of reaction under investigation [3, 20]. One of the most researched mixed phase titania is Degussa (Evonik) P25, with a blend of ~75%

anatase and ~25% rutile. Whether comparing pure or mixed phase titania, photoactivity is dependent upon i) the photocatalyst's response to light absorption and charge transport, ii) the surface response to charge trapping and transfer and iii) the surface chemical response to adsorbates involved in the electron transfer reactions [20].

Researchers have studied the surface reducibility of anatase and rutile to elucidate how the surface responds to charge carriers. They found that rutile was more easily reduced than anatase leading to the belief that rutile can serve as an electron sink or stabilize the surface charge in mixed phase systems [20, 43]. However, as a pure phase, rutile tends to exhibit high recombination rates resulting in lower photocatalytic activity in comparison to anatase [15, 24]. Further, anatase has shown a higher adsorptive affinity for organic compounds [7, 15, 24].

The band gap of rutile is 3.0 eV and anatase is 3.2 eV. The difference is primarily due to the position of the conduction band edge which is ~0.2 eV higher for anatase [44, 45]. Offsets in band alignment provide favorable conditions for electron transfer and facilitate charge separation at anatase-rutile interfaces [20, 24-26]. The smaller band gap of rutile leads to light absorption by excitation wavelengths that extend into the visible spectrum [24]. Band structure, and thus light absorption, may also be influenced by the extent of crystallinity, grain size, and impurities (e.g. dopants) [15]. Additionally, these physical parameters may modify charge recombination, trapping, and transport [15, 20].

1.3 Aqueous Organic Pollutants

1.3.1 Methyl Orange

Sodium 4-[(E)-[4-(dimethylamino)phenyl]diazenyl]benzenesulfonate ($C_{14}H_{14}N_3NaO_3S$), more commonly referred to as methyl orange (Fig. 3), is an azo dye. Azo dyes are frequently utilized in the textile industry and can be released into the environment in effluent streams [11].

They are water soluble, chemically stable, and resistant to biological and aerobic degradation [11, 46]. A number of investigations have been reported on the photocatalytic degradation of methyl orange [11, 16, 36, 38, 46-50]. Methyl orange is clearly visible, even at concentrations as low as 1 ppm, and readily quantified using UV-Vis spectroscopy. Due to its stable nature and ease of quantification, methyl orange is frequently used as a model pollutant for comparative studies of photocatalytic systems.

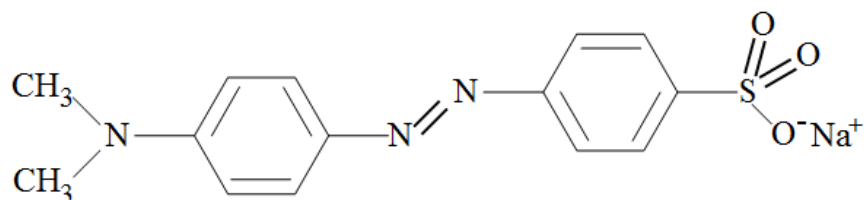


Figure 3 Molecular Structure of Methyl Orange

1.3.2 Geosmin and MIB

Trans-1,10-dimethyl-trans-9-decalol (geosmin) and 2-methylisoborneol (MIB) are semi-volatile, alicyclic tertiary alcohols. The molecular structures of geosmin (C₁₂H₂₂O) and MIB (C₁₁H₂₀O) are depicted in Figure 4. They are secondary metabolites produced by cyanobacteria and actinomycetes, and they cause musty and earthy flavors and odors in potable water and freshwater fish. They have reported human detection thresholds of 4 ng/L (ppt) for geosmin and 15 ng/L (ppt) for MIB [51]. They are non-toxic; however, issues with poor taste and smell often lead to consumer rejection. Further, they may be indicators of the presence of other more dangerous cyanobacteria byproducts, such as toxic microcystins.

Geosmin and MIB are lipophilic in nature and rapidly accumulate in fish flesh and roe. They can cause significant delays in harvesting and increase production costs. A variety of treatment methods have been explored for their removal from aqueous systems. Phase transfer

methods utilizing activated carbon [1, 52, 53] and zeolites [54, 55] as adsorbents have been examined. Adsorbents can be effective but may be limited due to the competitive effect of other organics in the water, the short life span of the adsorbent, disposal of spent adsorbents, and other operational concerns [56, 57]. Ultrasonic [58] and photolytic [59] degradation have also been explored. However, the most promising methods involve oxidation, with advanced oxidation processes having the highest removal rates [1].

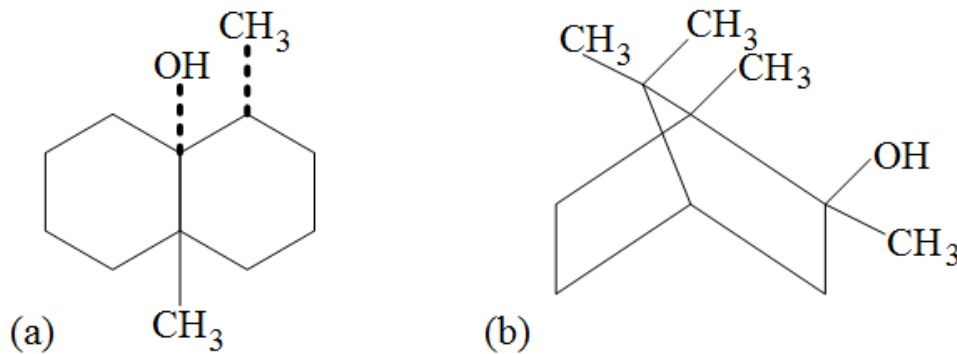


Figure 4 Molecular Structures of (a) Geosmin and (b) MIB

1.4 Aquaculture

Aquaculture is the cultivation of freshwater or saltwater species under controlled conditions. Species include fish, crustaceans, mollusks, and aquatic plants. In 2011, aquaculture supplied 63.6 million tonnes of fish, out of the 154 million tonnes consumed worldwide [60]. In Florida, aquaculture products accounted for \$69 million in 2012 revenues [61].

Sturgeons are one of the freshwater species cultivated in Florida's aquaculture industry. MOTE Marine Laboratory Aquaculture Research Park (MOTE MAP) in Sarasota has been cultivating sturgeon since 1997 in a recirculating aquaculture system (RAS). To recirculate water in RAS, several water treatment steps must be utilized to filter and chemically/biologically

treat the effluent from the fish culture tanks. A schematic of the primary water treatment system is detailed in Figure 5.

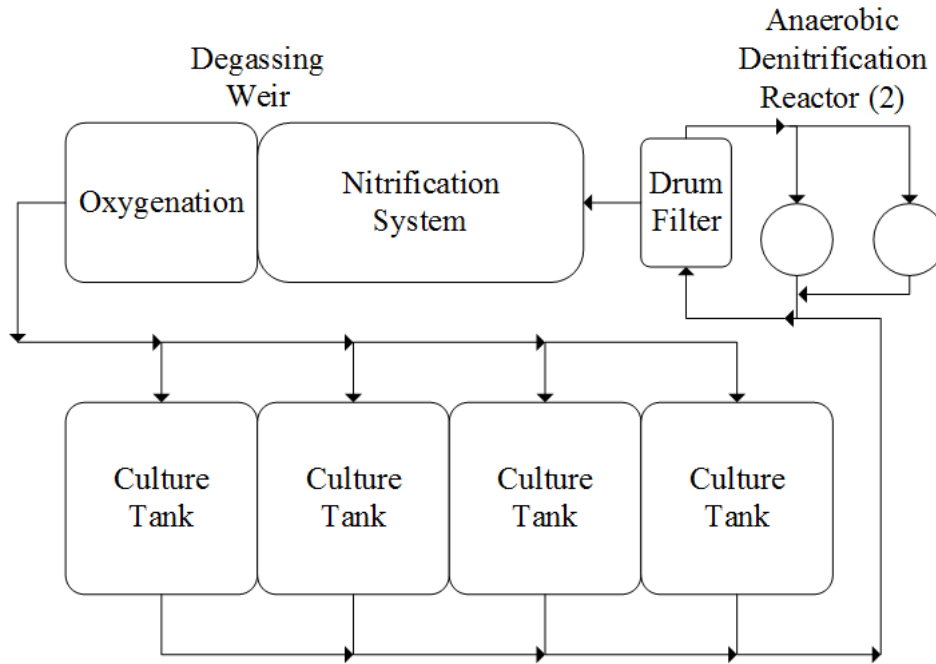


Figure 5 Schematic of Water Treatment at MOTE MAP

Sturgeons live and grow in fish culture tanks (Fig. 6). The culture tanks are arranged in groups, with each quadrant having a separate effluent treatment system. Effluent is drawn from the center, bottom of each culture tank and passed through a particulate filter (Fig. 7). From the filter there is a primary stream that enters the nitrification reactor system and a smaller slipstream that enters the anaerobic denitrification reactor.

In the nitrification system (Fig. 8), plastic media are used to grow bacteria that oxidize ammonia (aqueous waste product from fish). Ammonia (NH_3) is aerobically oxidized into ammonium (NH_4^+), then nitrite (NO_2^-), and finally nitrate (NO_3^-). The nitrification process consumes alkalinity and may lower the water pH. The removal of nitrate is accomplished in the anaerobic denitrification reactor (Fig. 9). Due to the anaerobic condition requirement, a

slipstream is taken from the drum filter versus the nitrification system. Bacteria, in this packed bed reactor reduce nitrate to dinitrogen (N_2).



Figure 6 Fish Culture Tanks



Figure 7 Drum Filter



Figure 8 Nitrification System



Figure 9 Anaerobic Denitrification Reactor

After passing through the nitrification system, water flows over a degassing weir (Fig. 10) and into the final compartment of the water treatment system. In this compartment (Fig. 11), oxygen generators are utilized to bring dissolved oxygen content near the saturation point. Further, water pH adjustments can be made by the addition of a base (e.g. sodium bicarbonate). Processed water is then pumped back into the culture tanks.

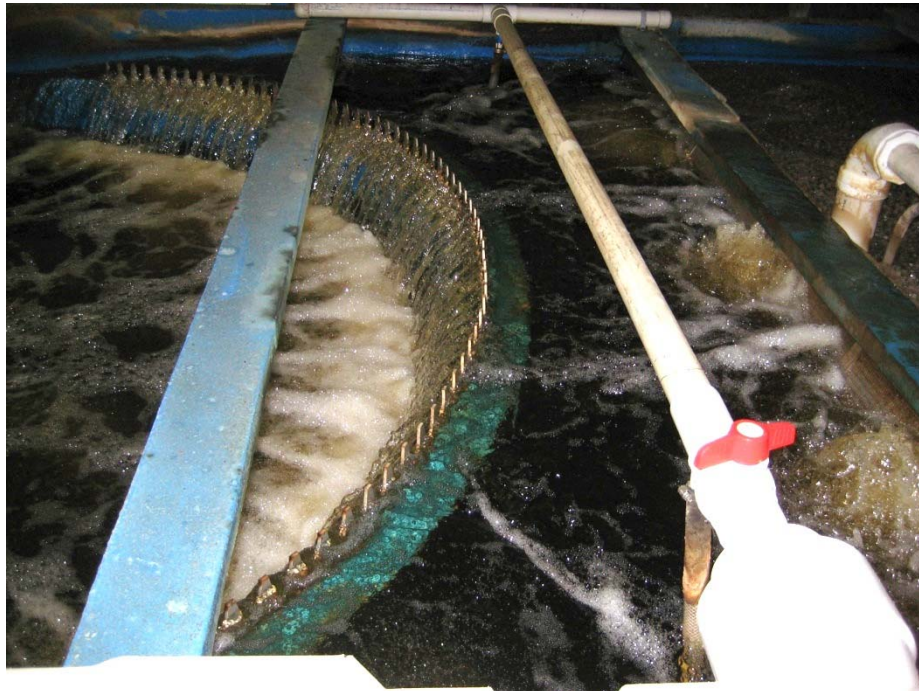


Figure 10 Degassing Weir

Juvenile sturgeons spend approximately 3 years in the culture tanks until they can be ultrasonically sexed. Male sturgeons are sold for fillets, while females require an additional 2-3 years of rearing before they produce roe. After roe extraction, females are also sold for fillets and the roe is processed into caviar. Due to the significant differential in product value, caviar is the primary product. Before the fillets or roe can be harvested, the sturgeon must undergo additional processing to reduce geosmin and MIB content. First, sturgeons are transferred from the culture tank to a purge tank (Fig. 12). The purge tank uses freshwater to drive the geosmin

and MIB via a concentration gradient out of the fish flesh and roe. Males will spend ~6 weeks in the purge tank and females will spend ~8 weeks due to the higher lipid content of the roe. During this time, large volumes of freshwater make-up, granular activated carbon, and/or ozonation may be used to remove geosmin and MIB from the water in the purge system. Each approach has limitations / drawbacks. Available freshwater is limited by aquifer constraints and environmental permitting restrictions. Granular activated carbon can be expensive to purchase, handle, and dispose. Ozonation rates are limited by fish health, as ozone residuals can cause gill adhesions and death. In addition to these concerns, female sturgeon may reabsorb the roe due to stress from the tank relocation and changes in feed rates; resulting in the loss of the primary product.



Figure 11 Oxygenation Compartment

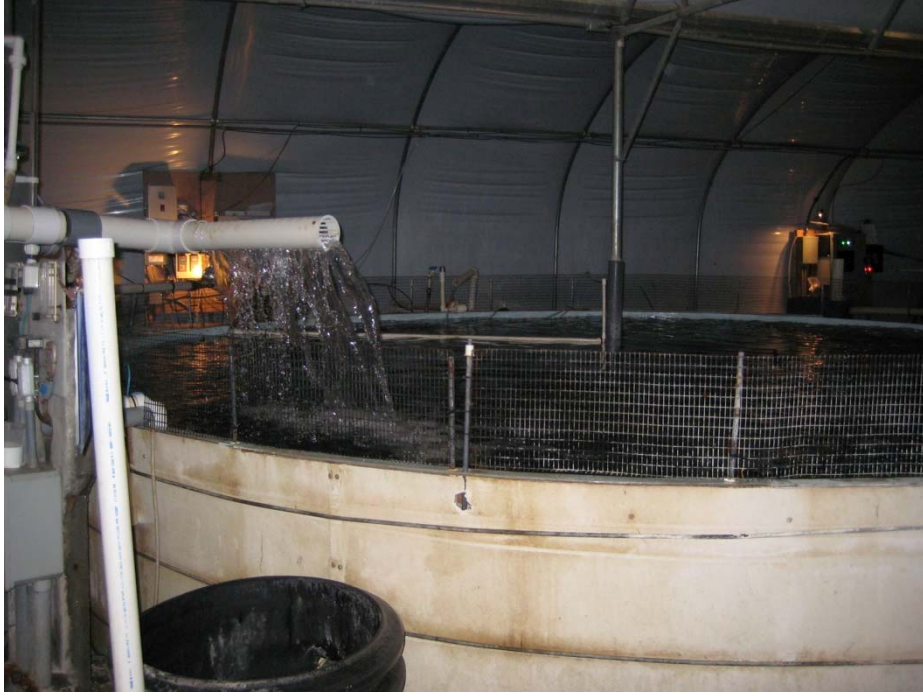


Figure 12 Purge Tank

CHAPTER 2: EXPERIMENTAL METHODOLOGY

2.1 Syntheses

2.1.1 Synthesis of InVO_4

Based upon the desired orthorhombic crystal structure, indium vanadate (InVO_4) was synthesized utilizing a modified precursor method where freshly precipitated indium hydroxide ($\text{In}(\text{OH})_3$) was combined with vanadium oxide (V_2O_5) using a chelating agent. Freshly precipitated $\text{In}(\text{OH})_3$ is significantly more reactive than commercially available $\text{In}(\text{OH})_3$ [62]. In a manner similar to the method presented by Zhang et al. [62], 5 g of indium (III) oxide (In_2O_3) was dissolved in 30 mL of 37% hydrochloric acid (HCl) at 65°C under magnetic stirring at 600 rpm. Once the In_2O_3 was completely dissolved, 30 mL of ammonia (NH_3) was slowly added in 3-5 mL increments. $\text{In}(\text{OH})_3$ forms as a white precipitate, which is separated from the supernatant and washed several times with distilled water. All reactions are carried out under the fume hood due to the rigorous nature of the reactions and the release of gas.

Diethylene triamine pentaacetic acid (DTPA) was used as a chelating agent for the next reaction sequence. The molecular structure of DTPA ($\text{C}_{14}\text{H}_{23}\text{N}_3\text{O}_{10}$) is shown in Figure 13. The required amount of DTPA is 1.6 moles DTPA to 1 mole $\text{In}(\text{OH})_3$. DTPA, with 30% excess, was dissolved in 50 mL of distilled water at 85°C . V_2O_5 is measured at a ratio of 1 mole V_2O_5 to 2 moles $\text{In}(\text{OH})_3$. The stoichiometric amounts of V_2O_5 and $\text{In}(\text{OH})_3$ were simultaneously added to the hot DTPA solution. The resulting slurry underwent several color changes. Once it became bright blue, the stir rod was removed. The viscous solution was allowed to crystallize in air

under ambient conditions. The brittle, glasslike crystal was then ground into a fine powder using a mortar and pestle. The powder was calcined in stagnant air at 600°C for 400 minutes with an initial ramp rate of 3°C/min.

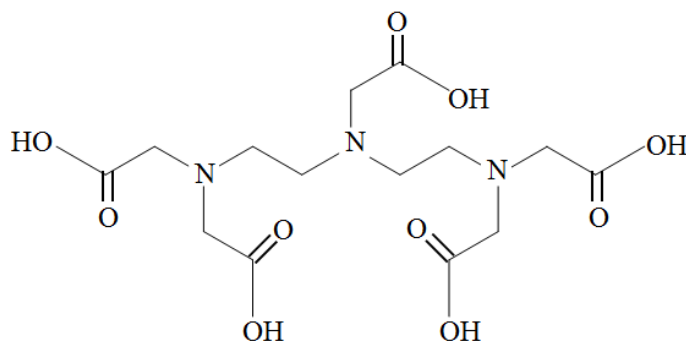


Figure 13 Molecular Structure of DTPA

Fourier Transform Infrared Spectroscopy (FTIR) was utilized to analyze the powders before and after calcination. Before calcination, the indium-vanadium-DTPA complex produced a spectrum (Fig. 14) displaying a variety of H stretching (C-H and O-H) in the 3600-2500 cm^{-1} range and aliphatic C-N stretching in the 1370-1000 cm^{-1} range. The fingerprint region also contained other peaks characteristic of C-H bending and carboxylic acid vibrations.

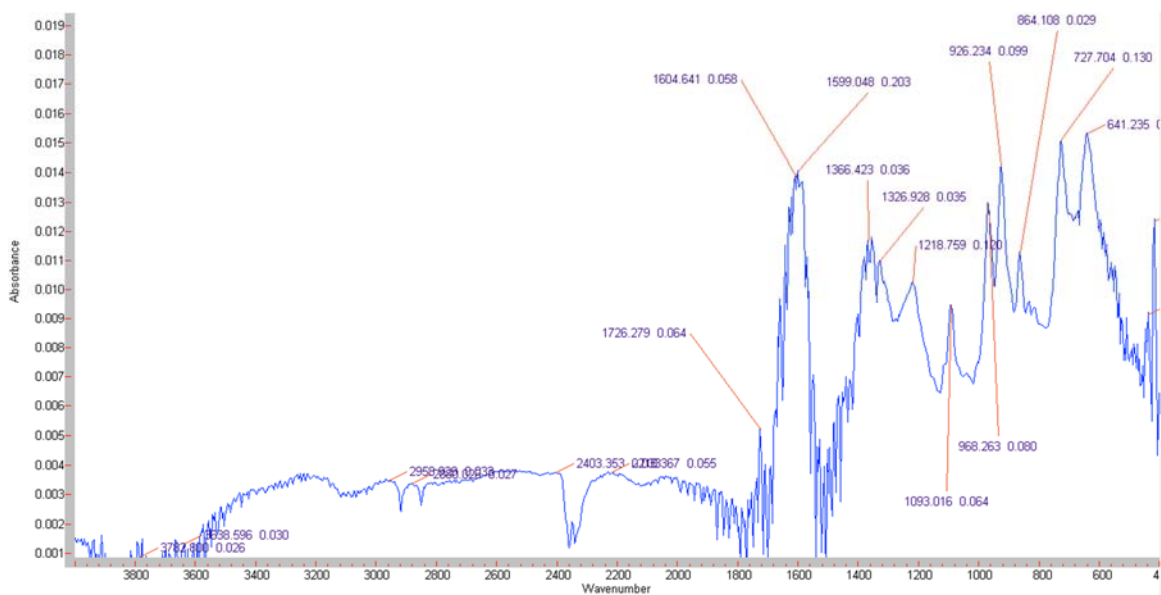


Figure 14 FTIR Spectrum of Indium-Vanadium-DTPA Complex

After calcination, the powder was salmon-tan in hue. The FTIR spectrum (Fig. 15) shows strong peaks at 898 and 699 cm^{-1} . These peaks have been identified with terminal V-O stretching and V--O--In bridging, respectively [63]. No evidence of carbon or nitrogen bonding is observed, indicating that all of the organic material was successfully removed by calcination.

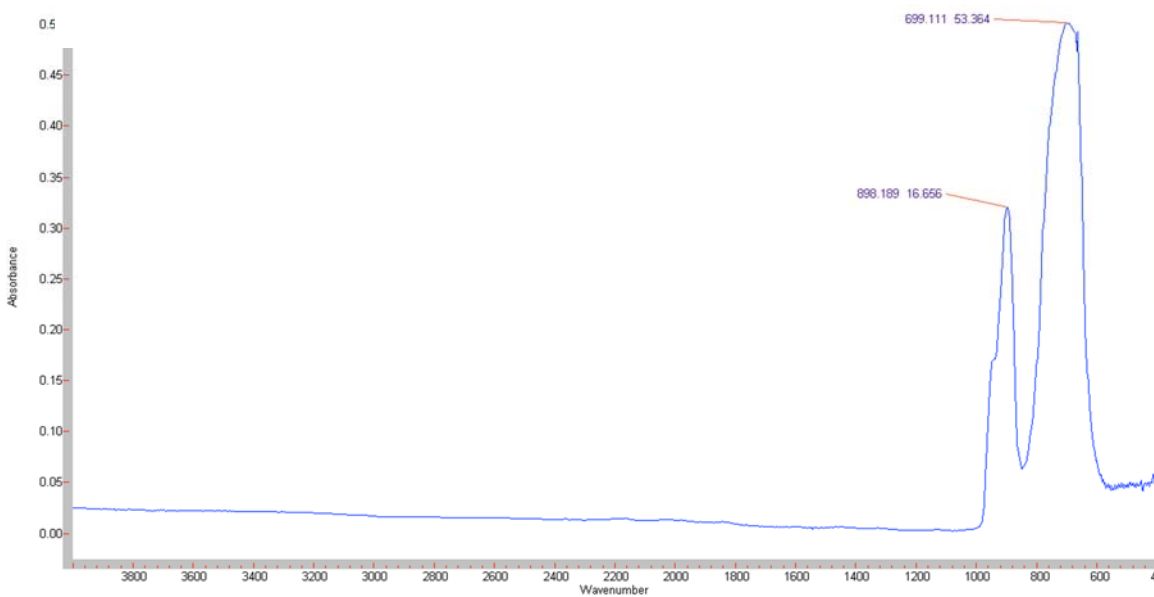


Figure 15 FTIR Spectrum of InVO₄ Powder (Post Calcination)

InVO₄ may exist in amorphous or crystalline form. The orthorhombic crystal structure displays photocatalytic properties [36, 48, 62, 64-69] and is the desired polymorph for this work. The XRD stick pattern of the as-synthesized InVO₄ was compared to the Joint Committee on Powder Diffraction Standards, JCPDS reference card 00-048-0898 (InVO₄, orthorhombic, space group Cmc₂m, no. 63) in Figure 16. The pattern correlated with the orthorhombic reference card with the highest signal at a 2-theta position of 33°.

Composition and morphology of the as-synthesized InVO₄ was elucidated via SEM and EDS. Figure 17 shows a grain-like structure with typical particle sizes of 1-2 μm . The shape is similar to orthorhombic InVO₄ formed via high temperature solid-state reactions. However, the

solid-state synthesis method forms slightly larger particles, approximately 5-6 μm [66]. High resolution SEM (at 25 kV accelerating voltage) was not possible without manipulation of the sample (e.g. Au coating) due to surface charging of the semiconductor. EDS analysis, shown in Figure 18, indicates characteristic oxygen, indium, and vanadium emissions (note that the sample is mounted on an aluminum stage).

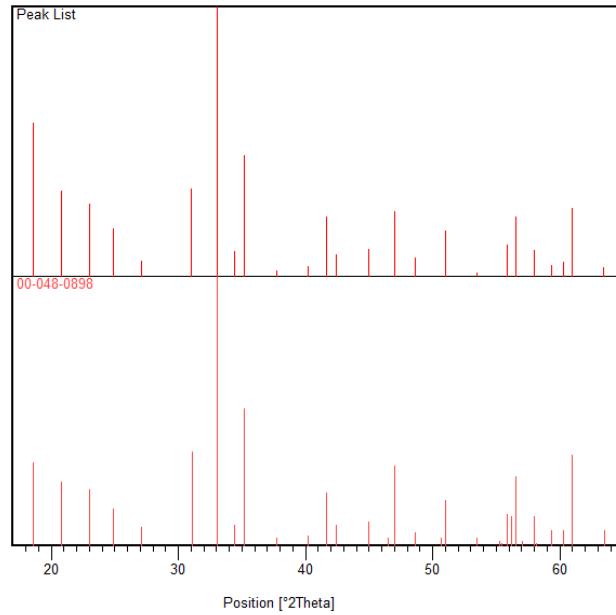


Figure 16 XRD Stick Patterns of Synthesized and Orthorhombic Reference InVO_4

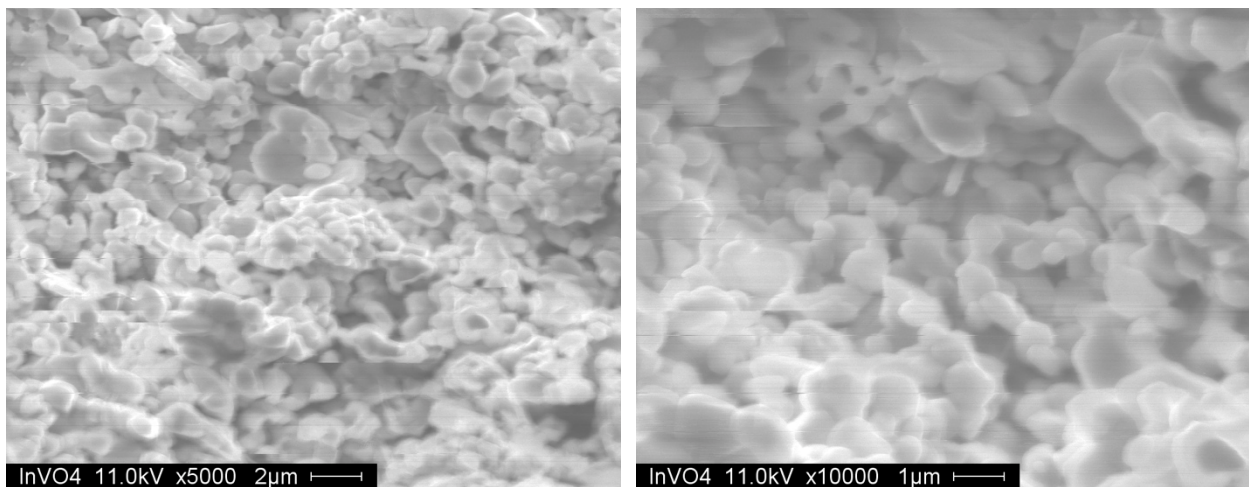


Figure 17 SEM Images of InVO_4 at 5k and 10k Magnification

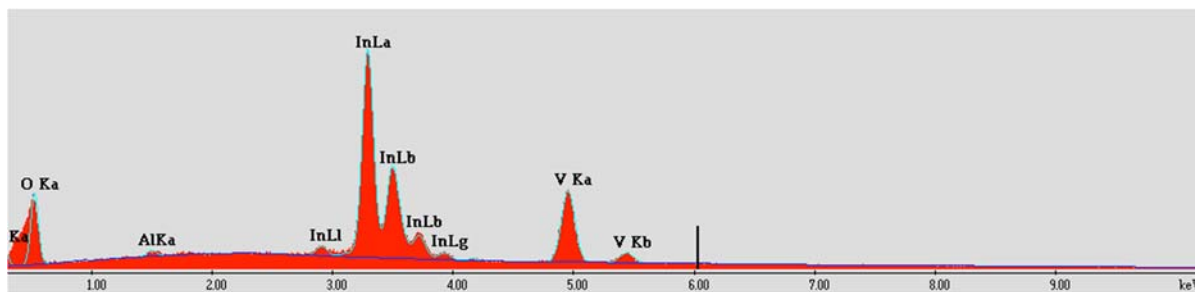


Figure 18 EDS Spectrum of Synthesized InVO₄

2.1.2 Synthesis of InVO₄-TiO₂ Composites

Previously reported work performed with InVO₄-TiO₂ composites [36, 47-49, 64, 65] utilized a combination of InVO₄ sol and peroxy titanate acid (PTA) sol to prepare dip coated substrates. The PTA sol method produces anatase phase titania [70]. Anatase can be converted to rutile through thermal treatment; however, the thermal treatment also results in loss of surface area and sintering [20]. To avoid these unwanted consequences, amalgamation of the two semiconductors was achieved through mechanical grinding. Various weight ratios of InVO₄ powder were combined with anatase, rutile, and P-25 titania powders. The dry powders were mixed with a spatula and then ground for 15 min in ~5 g batches in an agate mortar and pestle. Mulling agents were not used and a nylon bristle brush prevented agglomeration on the mortar and pestle. Detailed characterization of the InVO₄-TiO₂ composites is presented in Chapter 3 and Figure C-1 in the Appendix. The surface area, determined by the Brunauer-Emmett-Teller (BET) method using a Quantachrome Autosorb IQ, was 58 m²/g; and the pore volume was 0.073 cc/g with an average pore diameter of 5 nm.

2.2 Characterization

2.2.1 Fourier Transform Infrared Spectroscopy

A Bio Rad Excalibur FTS 3000 spectrometer (Fig. B-1) was utilized to collect FTIR spectra. The spectrometer was equipped with a PIKE attenuated total reflectance (ATR) sample

holder with a diamond crystal (Fig. B-2). The system was operated at 20 kHz with 4 cm⁻¹ resolution and 128 scans per sample. DigiLab software performed the necessary transforms and utilized Norton-Beer Medium apodization.

2.2.2 X-ray Diffraction

A Philips PANalytical X-pert Pro X-ray Diffractometer was used to generate powder X-ray diffraction (XRD) patterns for synthesized and as-procured samples. The instrument was operated with Cu K α radiation ($\lambda = 0.154$ nm), a 45 kV accelerating voltage, and 40 mA applied current. Reported XRD pattern noise was reduced using HighScore software developed by PANalytical.

2.2.3 Scanning Electron Microscopy and Energy Dispersive X-ray Spectroscopy

A Hitachi S-800 scanning electron microscope (SEM) equipped with EDAX energy dispersive X-ray spectroscopy (EDS) was utilized to elucidate morphology and composition. Images and spectra were acquired using an accelerating voltage from 10 to 20 kV. Samples were fixed via carbon tape or applied pressure to an aluminum stage. Copper conducting tape was utilized to minimize charge accumulation on the semiconductor samples. Elemental maps were prepared based upon titanium (K $\alpha = 4.5$ keV) and indium (K $\alpha = 3.3$ keV). Vanadium was not mapped due to the overlap in energy of its K α emission with the titanium K β emission.

2.3 Quantification and Measurement

2.3.1 Methyl Orange

Methyl orange was utilized as a model pollutant to perform various parametric and kinetic studies with a batch slurry reactor. The slurry samples (Fig. 19) were separated by an Eppendorf 5415C Centrifuge (Fig. B-4) at 8000 rpm for 15 min. Decanted solutions were analyzed in plastic 1.5 mL cuvettes. Concentration was calculated based upon absorbance

measured by a Perkin Elmer Lambda 35 UV-Vis Spectrometer (Fig. B-3). Absorbance was measured from 375 to 575 nm with a 60 nm/min scan rate. Figure 20 shows that methyl orange has a broad absorbance peak centered near 465 nm. Using the Lambert-Beer Law, absorbance can be linearly correlated with methyl orange concentration.



Figure 19 Centrifuged Methyl Orange Aliquots

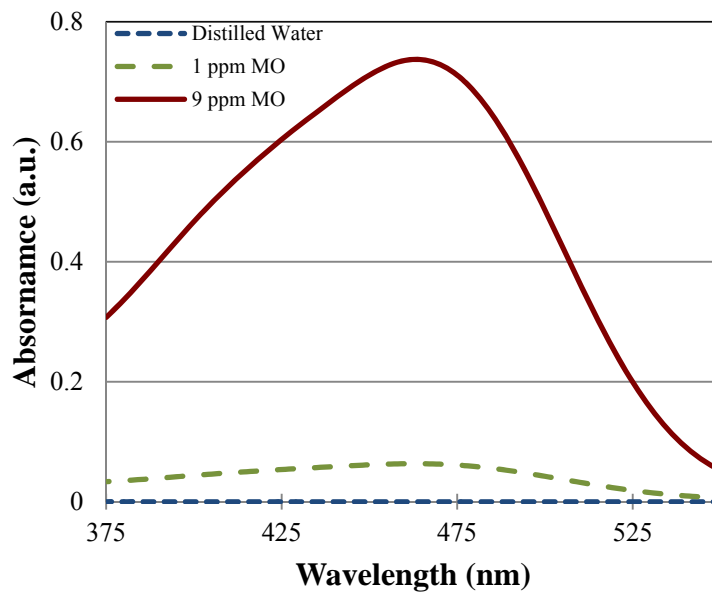


Figure 20 UV-Vis Absorbance of Methyl Orange

2.3.2 Geosmin and MIB

Detection and quantification of geosmin and MIB at trace levels (in the range of 10 ppt) in aqueous systems require the use of a selective and sensitive method. Historically, many techniques have been examined, each with specific limitations. Closed loop stripping followed by gas chromatography – mass spectrometry (GC-MS) effectively isolates geosmin and MIB but requires sample processing in excess of 3.5 h [71]. Liquid-liquid extraction requires large sample volumes and intensive sample preparation [72]. Membrane-assisted solvent extraction (MASE) is expensive, requiring cryogenic coolants and consumable membranes and magnets [73].

During the last decade, researchers have shifted to a headspace solid-phase microextraction (SPME) technique followed by GC-MS analysis for the detection of trace amounts of geosmin and MIB [39, 56, 58, 59, 74, 75]. The American Water Works Association Method 6040D provides SPME guidelines for several taste and odor producing compounds [76]. A modified method 6040D was utilized in the quantification of geosmin and MIB.

The SPME technique uses a flexible fiber coated with a suitable adsorbent and bound to the tip of a plunger inside a hollow needle. The needle pierces the septum of a sample vial and then the fiber is extended into the headspace of the vial to adsorb analytes. A complete SPME assembly is detailed in Figure 21. In the analysis of geosmin and MIB, a divinylbenzene / carboxen / polydimethylsiloxane (DVB/CAR/PDMS) fiber is utilized.

Aliquots of 30 mL were collected in PTFE-faced septum, screw-cap 40 mL glass vials. 2-isobutyl-3-methoxypyrazine (IBMP) at a concentration of 100 µg/L was used as an internal standard. Sodium chloride (9 g), previously baked at 500°C for 5 h, and IBMP (3 µL) were added to the sample vial. Vials were immersed in a 60-65°C water bath and continuously stirred

with a magnetic PTFE coated stir bar. The SPME holder (Supelco manual holder, part 57330-U) was set to 0.8 to adjust needle length for piercing of the septum. The SPME fiber was extended (to the first holder notch) into the headspace above the liquid surface. After 30 min of adsorption time, the fiber was retracted and transferred to the GC injector.

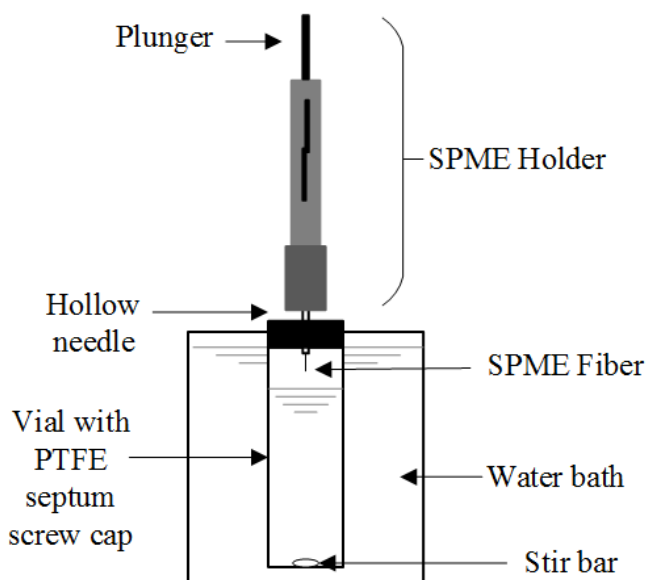


Figure 21 SPME Assembly

Before insertion into the GC injector, the holder was adjusted to a setting of 3.6 to ensure that the needle would pierce the injector septum and protect the fiber. Once fully extended, the fiber remained in the injector for 3 min to thermally desorb the analytes at 250°C. Helium was utilized as the carrier gas (1 mL/min) and for split flow of 50 mL/min, after 2 min of initial splitless operation. A Perkin Elmer Clarus 580 GC (Fig. B-5) equipped with a 30 m x 0.25 mm x 0.25 μ m HP-5MS column (Agilent J&W) separated the analytes using a temperature program from 50°C (held for 1 min) to 280°C (held for 1 min) via a ramp rate of 15°C/min. The GC-MS interface temperature was set at 280°C. A Perkin Elmer Clarus 560D MS was operated in

Selective Ion Monitoring (SIM) mode for quantification of analytes. The MS utilized electron ionization with a source temperature of 200°C and span of 0.5 daltons.

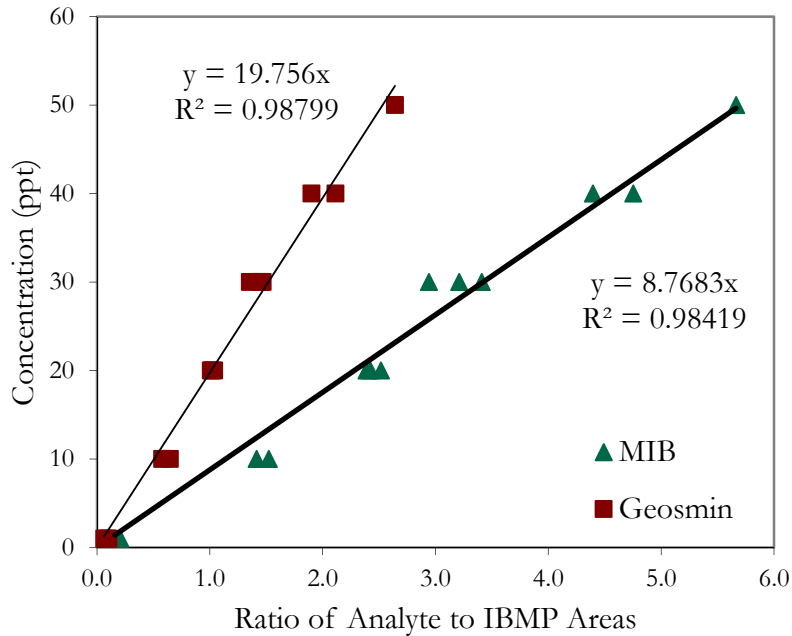


Figure 22 Calibration Curves for Quantification of Geosmin and MIB

A series of geosmin and MIB solutions were prepared at concentrations of 1, 10, 20, 30, 40, and 50 ng/L (ppt). SPME analysis was performed after spiking each sample with IBMP (IBMP final concentration held constant at 10 ng/L). IBMP, MIB, and geosmin eluted at approximately 7.3, 7.4, and 9.5 min. The chromatograph peaks, minus the baseline, were numerically integrated using the trapezoidal rule to determine the area under each peak. The ratio of analyte area to IBMP area was plotted against the known concentrations to develop calibration curves (Fig. 22). During each experimental run, a calibration check was performed to ensure fiber performance.

An analysis of the detection limits was performed using a series of seven 1 ppt geosmin and 1 ppt MIB samples. The method detection limit was calculated with a t value of 3.14 for a

99% confidence interval. The results are tabulated in Table 1. The practical quantification limit was computed as five times the method detection limit.

Table 1 Geosmin and MIB Detection Limits

	MIB	Geosmin
Average (ppt)	0.9	1.0
Standard Deviation	0.27	0.11
Method Detection Limit (ppt)	0.8	0.3
Practical Quant. Limit (ppt)	4	2

2.4 Photoreactor

2.4.1 Batch Slurry Reactor

Initial experiments were conducted in a continuously stirred 1 L Pyrex batch slurry reactor (Fig. 23) enclosed in an aluminum housing with black interior walls (Fig. 24). The radiation source was five General Electric T5F8 (12 inch mini bi-pin) 8 watt fluorescent bulbs. Daylight spectrum bulbs with a Color Rendering Index of 75 were utilized for visible light experiments, and Blacklight Blue spectrum bulbs emitting at a peak wavelength of 368 nm were utilized for ultraviolet experiments. Daylight bulbs have a color temperature of 6500 K and reported luminous flux of 265 lumens. The spectral irradiance measured at 9 cm (approximate distance to fluid surface) by a Li-Cor pyranometer was 60 W/m².

Parametric studies were conducted to determine operating conditions for the batch slurry system. Figures and data related to these studies can be found in the supplemental data in Appendix C. Catalyst dosing (i.e. the ratio of catalyst weight to aqueous volume) was analyzed at 0.5, 0.75, and 1.0 g/L. The rate of methyl orange degradation increased with increased catalyst dosing (Fig. C-3). Our partners at the King Abdulaziz University (KAU), Saudi Arabia, performed a similar experiment using a 150 W visible spectrum halide lamp. Approximately 80 g of 2% InVO₄-TiO₂ was prepared for KAU for the decomposition of 2-chlorophenol. Catalyst



Figure 23 Batch Slurry Reactor



Figure 24 Photoreactor Enclosure

dosing rates of 0.1, 0.25, 0.5, 1.0, and 2.0 g/L were evaluated. 2-Chlorophenol degradation was maximized at 1.0 g/L. Dosing higher than 1.0 g/L resulted in a drop in degradation due to reduction in light penetration and possible agglomeration of the photocatalyst.

The magnetic stirring rate was varied between 125 rpm and 350 rpm and had only a slight impact on photocatalytic degradation (Fig. C-4). A rate of 250 rpm provided the best results and was utilized for the remainder of the batch system scenarios. Weight ratio of InVO₄ to TiO₂ was reviewed in the 1% to 10% range. Although 5% InVO₄ composites are used to present characterization findings, the 2% InVO₄ composite displayed a slightly higher methyl orange degradation rate (Fig. C-5).

2.4.2 Flow Reactor

In the batch slurry reactor, the powder catalyst was separated from the slurry using centrifugation. In scaled application, this type of separation process would increase the cost and pose significant operational concerns. To develop a scalable system, immobilization of the photocatalyst is required. Here, titania was immobilized on borosilicate glass plates utilizing a spray coating technique.

The 1/8 in (0.31 cm) glass was cut into 2 in (5.1 cm) x 7 in (20.3 cm) plates and cleansed with ethanol. The plates were hung vertically inside a fume hood against an aluminum foil backdrop with a delineated spray zone. The area of the spray zone was used to determine the catalyst weight with a target immobilized concentration of 0.25 mg/cm² (20% system loss was assumed). Ethanol (95%) was added to the catalyst at a ratio of 20 mL to 1 g, and the slurry was mixed for 15-20 sec using a vibratory plate. A Paasche HAPK H#3 airbrush, at a distance of ~6 in (15 cm), was used to evenly coat the entire spray zone with the catalyst slurry. Catalyst was

allowed to dry under ambient conditions for 1 hr. Plates were then transferred to an oven with a stepped temperature profile of 1.5 h at 100°, 0.5 h at 200°, and 2 h at 500°C.

The plates were placed in the bottom of a shallow reactor. The reactor vessel was fabricated from reflective aluminum sheet metal with dimensions of 15 in (38.1 cm) long by 2 in (5.1 cm) wide by 1 in (2.5 cm) high. The vessel cover contained a housing for two 8-watt F8T5 fluorescent bulbs (Fig. 25). To mimic a recirculating aquaculture system, a 5 L aspirator bottle was used as a reservoir. Effluent was pumped via a peristaltic pump at 180 mL/min to the reactor where it flowed in sheets over the catalyst coated glass plates. The system is detailed in Figure 26.



Figure 25 Flow Reactor with Removed Cover

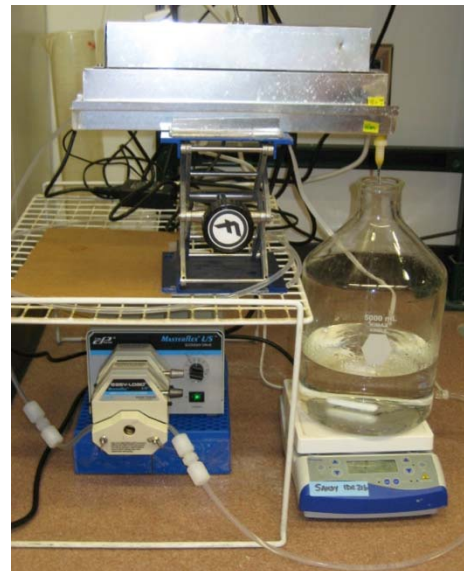
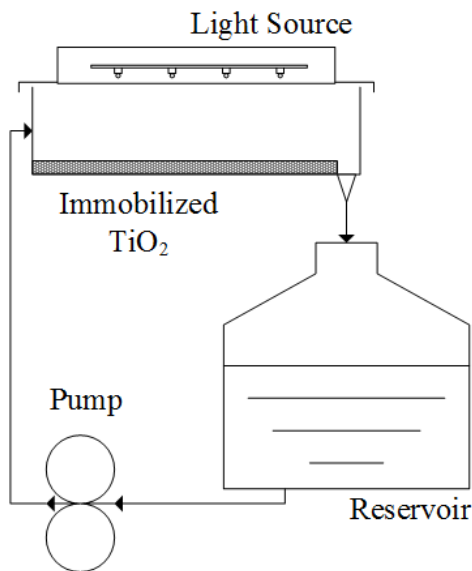


Figure 26 Flow Reactor System

CHAPTER 3: PURE AND MIXED PHASE TITANIA COMPOSITES¹

3.1 Introduction

Advanced oxidative processes, including photocatalysis with titanium dioxide (TiO₂), have shown significant potential for the treatment of wastewater and potable water [1]. TiO₂ is an effective, inexpensive, and stable photocatalyst used for the decomposition of organics. With a band gap of 3.0-3.2 eV, photoinitiation of TiO₂ occurs primarily in the ultraviolet portion of the spectrum. Shifting photoinitiation further into the visible spectrum may provide more sustainable solutions to current water processing technologies.

Photocatalytic properties of TiO₂ have been widely studied over the last few decades. A compilation of data, principles and mechanisms related to early work was prepared by Linsebigler et al. [42]. A more topical summary prepared by Henderson, focuses on charge transport and trapping, promoters, and the effect of phase and form [20]. In recent years, attempts have been made to increase photocatalytic activity and/or to move the photo-initiation into the visible spectrum by utilizing a dopant or composite material. Experimental dopants have included metal ions [5] and non-metals such as nitrogen [27-29], carbon [30], or sulfur [13]. Composite materials have been synthesized by coupling TiO₂ with other semiconductors such as AgBr [12], Ag₃PO₄ [77], CdS [42], InVO₄ [36], and WO₃ [17, 32]. Due to cost and stability issues, silver (and other noble metal) composites are limited in their practical application [77].

¹ This chapter was published in *Catalysis Letters* (S. Pettit, C. McCane, J. Wolan, J. Kuhn, *Synthesis, Characterization, and Photocatalytic Degradation Performances of Composite Photocatalytic Semiconductors (InVO₄-TiO₂) Using Pure and Mixed Phase Titania Powders*, *Catal. Lett.*, 143 (2013) 772-776.

Metal oxides can provide a variety of photocatalytic enhancements, from new interfacial reaction sites; to electron scavenging and storage sites; to charge carrier generation, separation, and transfer [20]. InVO₄ has been shown to have four sub-bandgap transitions, of which three are in the visible range [2]. Several studies have shown promising results for visible light initiation of InVO₄-TiO₂ films for the photocatalytic decomposition of aqueous organics [48, 49, 64]. For these reasons, InVO₄ was chosen for the composite material for this work.

A number of InVO₄ synthesis methods have been reported, as outlined here. The synthesis method results in a specific phase and form, which in turn, dictates the functionality. Hydrothermal methods with organic additives have been used to synthesize specific shapes of InVO₄ nanoparticles for sensors [78]. Spray pyrolysis onto a substrate, used for thin film anodes, yields a mixture of monoclinic and orthorhombic phases [79]. Sol-gel synthesis and dissolution-precipitation methods have been demonstrated to produce amorphous InVO₄, which has a high charge capacity and can be used in electrochromic devices [63, 80]. Touboul et al. described the *chimie douce* process for synthesis of monoclinic and metastable crystals [81, 82]. Photocatalytically active orthorhombic InVO₄ films and powders have been synthesized from a complex precursor followed by calcination [62, 83].

The InVO₄ synthesis method, chosen for the current study, attempts to optimize properties for visible light photocatalysis for the destruction of aqueous organics. Previous research has indicated that visible light absorption is higher in InVO₄ powders than in thin films [79]. Further, orthorhombic powders prepared from a complex precursor method have shown photoactivity for formaldehyde decomposition [62].

Next, the formation of the composite InVO₄-TiO₂ must be addressed. One route utilizes the combination of InVO₄ sol and peroxy titanate acid (PTA) sol to prepare dip coated substrates

[49]. Two concerns arise from this method: i) the lower visible light absorption rate of films and ii) the product crystal structure. PTA sols are deposited as amorphous films and, after calcination, crystallize as anatase TiO_2 [37]. Although anatase crystals have traditionally been viewed as the most photoactive, recent research suggested that mixed phase titania may show greater photoactivity for some reactions [15, 20, 23, 24]. Whether there is a synergistic effect as proposed by some researchers [15, 23] or enhanced activity due to interfacial properties as proposed by others, [20, 24] the evidence indicated that the combination of anatase and rutile crystals is more effective than pure phase catalysts. A portion of anatase crystals can be transformed to rutile through annealing; however, particles may sinter causing loss of surface area and increase of particle size [7, 15, 20, 37].

Another route for the composite formation is mixing and grinding. High-energy ball milling of TiO_2 powders can induce phase transformations from anatase to TiO_2 II to rutile [33-35]. Since the mechanisms for phase transformation under high energy ball milling are not well understood and models frequently rely upon empirical data [34], a low energy approach was undertaken utilizing mortar and pestle. This letter demonstrates that a photoactive composite powder ($\text{InVO}_4\text{-TiO}_2$) is achieved through mechanical grinding and the dopant (InVO_4) is possible to be added to a single phase and mixed phase (P-25) TiO_2 powders without a phase change of the TiO_2 . This achievement is possible because calcination steps for the composites are avoided through the use of the mechanical grinding process, which still allows for the formation of a semiconductor-semiconductor interface. This method is envisioned to be a platform for the synthesis of other semiconductor composites, in addition to InVO_4 , for synthesis of composite photocatalysts with specific titania phases.

3.2 Experimental

3.2.1 Chemicals

Indium (III) oxide (In_2O_3 , 99.99%) and vanadium (V) oxide (V_2O_5 , 99.2%) from Alfa Aesar were used as precursors of indium vanadate (InVO_4). Mixed phase titanium dioxide (TiO_2) P-25 was procured from Evonik Degussa. Anatase TiO_2 (99.6%) and rutile TiO_2 (99.5%) were procured from Alfa Aesar. Hydrochloric acid (HCl, 37%), ammonia solution (10-35%), diethylene triamine pentaacetic acid (DTPA, 98+%) were reagent grade. Methyl orange ($\text{C}_{14}\text{H}_{14}\text{N}_3\text{SO}_3\text{Na}$) was certified ACS grade from Fisher.

3.2.2 Synthesis of InVO_4

Preparation of InVO_4 from freshly precipitated $\text{In}(\text{OH})_3$ was similar to Zhang's method [62]. A 5.0 g In_2O_3 sample was completely dissolved in 30 mL of HCl at 65°C under continuous magnetic stirring. Due to the rigorous nature of the reaction, ammonia solution was added slowly (in excess). $\text{In}(\text{OH})_3$ precipitated from the solution. The precipitate was separated and washed several times with deionized (DI) water.

With continuous stirring, 50 mL of DI water and 29.5 g of DTPA were heated to 85°C . The freshly prepared $\text{In}(\text{OH})_3$ precipitate and a stoichiometric amount ($\text{In}/\text{V} = 1/1$) of V_2O_5 were simultaneously added to the DTPA solution. The resulting slurry was bright blue. The slurry was air dried at room temperature to form a brittle, glasslike crystal. The crystal was ground using mortar and pestle to a fine powder. The powder was heated at a $3^\circ\text{C}/\text{min}$ ramp rate to 600°C , where it was calcined in stagnant air for 400 minutes.

3.2.3 Preparation of $\text{InVO}_4\text{-TiO}_2$ Composites

$\text{InVO}_4\text{-TiO}_2$ (P-25) powders were prepared with InVO_4 weight at 1, 2, 5 and 10 %. $\text{InVO}_4\text{-TiO}_2$ (A) and $\text{InVO}_4\text{-TiO}_2$ (R) were prepared at 5 wt% InVO_4 . Composites with less than

5 wt% InVO₄ had weak signals in some techniques; therefore, characterization of the 5 wt% composites is presented. The dry semiconductor powders, InVO₄ and TiO₂, were mixed with a spatula. Small batches, approximately 1-5 g, of mixed powders were ground with an agate mortar and pestle for 15 minutes. A nylon bristle brush was utilized to prevent agglomeration of the powder on the mortar. A milling agent or mulling oil was not required.

3.2.4 Characterization

Crystallographic information of the as procured and as prepared samples was analyzed by powder X-ray diffraction (XRD) using a Philips PANalytical X-pert Pro X-ray Diffractometer. The diffractometer used Cu K α radiation with a 45 kV accelerating voltage and 40 mA applied current. Morphology and composition were investigated via a Hitachi S-800 scanning electron microscope (SEM) equipped with EDAX energy dispersive X-ray spectroscopy (EDS). Secondary electron images were acquired using an accelerating voltage from 10 to 20 kV.

3.2.5 Photocatalytic Activity

Photocatalytic reactions were carried out in a 1 L Pyrex reactor at atmospheric pressure and ambient temperature, without pH buffering. General Electric T5F8 “Daylight Spectrum” (Color Rendering Index 75) 8 W fluorescent bulbs were utilized as the radiation source. Methyl orange at 9 ppm was utilized as the model pollutant. Catalyst was loaded at 1 g/L of solution, and suspended using magnetic stirring. Every 15 minutes, aliquots of 1.5 mL were drawn. The suspension was separated using an Eppendorf 5415C Centrifuge. Decanted solutions were analyzed in the 575 to 375 nm range using a Perkin Elmer Lambda 35 UV-Vis Spectrometer to determine the methyl orange concentration.

3.3 Results and Discussion

Prior to alloying of the semiconductors, characterization of the as-synthesized InVO_4 was performed. The XRD pattern (Fig. 27) indicated the presence of orthorhombic crystals and all observed peaks correlated with JCPDS 00-048-0898 (InVO_4 , orthorhombic, space group Cmcm , no. 63). No other phases or impurities were detected. The secondary electron image indicates that the InVO_4 powder is comprised of an agglomeration of smaller grain like structures, as shown in Figure 28, with a typical grain size of $\sim 1 \mu\text{m}$.

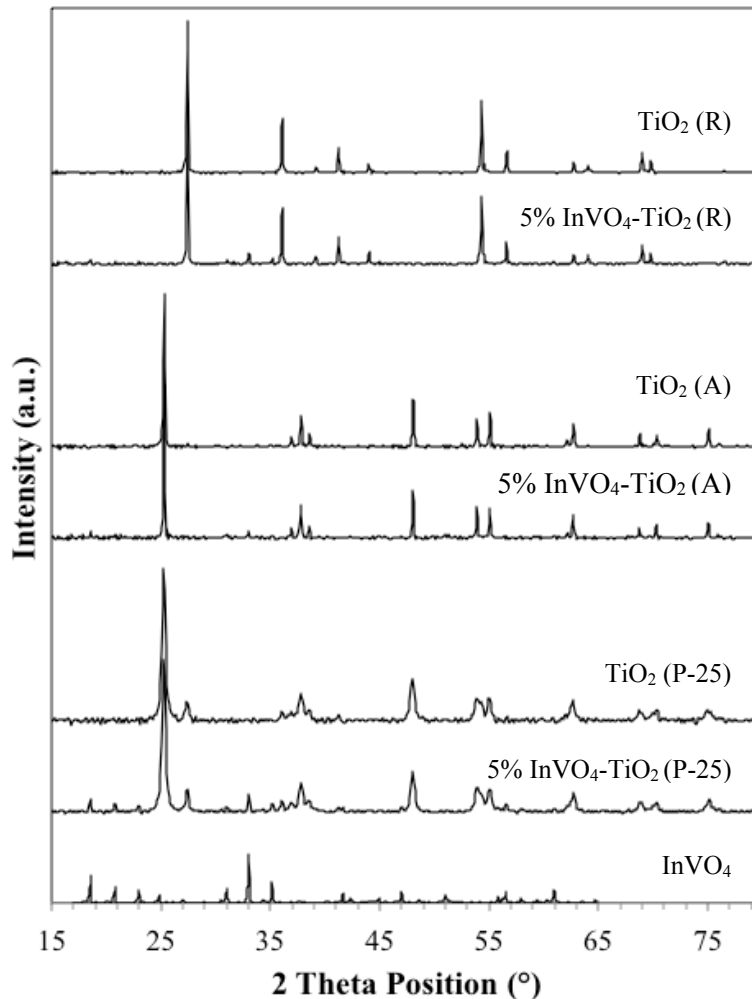


Figure 27 XRD Patterns of Synthesized InVO_4 , Pure and Mixed Phase TiO_2 , and InVO_4 - TiO_2 Composites

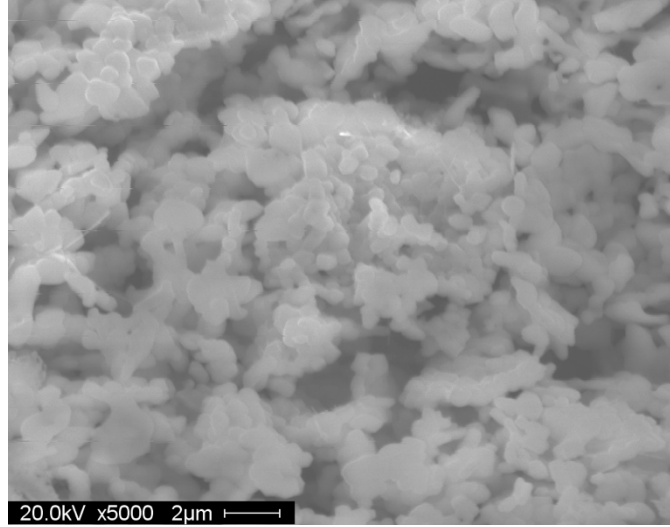


Figure 28 SEM Image of Synthesized InVO₄

The XRD patterns for the pure and mixed phase titania and their respective composites are also shown in Figure 27. The TiO₂ (R) pattern indicates the presence of tetragonal crystals and all observed peaks correlated with JCPDS 03-065-0191 (TiO₂ rutile, tetragonal, space group P42/mnm, no. 136). The TiO₂ (A) pattern correlated with JCPDS 01-071-1166 (TiO₂ anatase, tetragonal, space group I41/amd, no. 141). As expected, the mixed phase TiO₂ powders contained both anatase and rutile peaks (reference JCPDS 01-071-1166 and 03-065-0191). For the composite sample with mixed phase TiO₂, the relative intensities between anatase and rutile peaks showed no significant change, thus indicating that grinding did not induce a phase change in the TiO₂ crystals. Further, orthorhombic InVO₄ were observed in all composite materials at 18.5 and 33°.

Elemental mapping (from energy dispersive X-ray analysis) showed the successful dispersion of indium and titanium throughout the composite sample (Fig. 29). Mapping of vanadium would provide no beneficial value because of the lack of accuracy due to overlapping Ti K β and V K α peaks at 4.9 eV. In addition to the overlapping peaks, quantitative EDS analysis

is limited by lack of available calibration standards and the large excitation volume of TiO₂. The EDS spectrum of the composite is shown in Figure 30. Qualitatively, it indicated that no impurities are present. Further magnification shows that the InVO₄ is dispersed in 1-8 μm clusters, as shown in Figure 31.

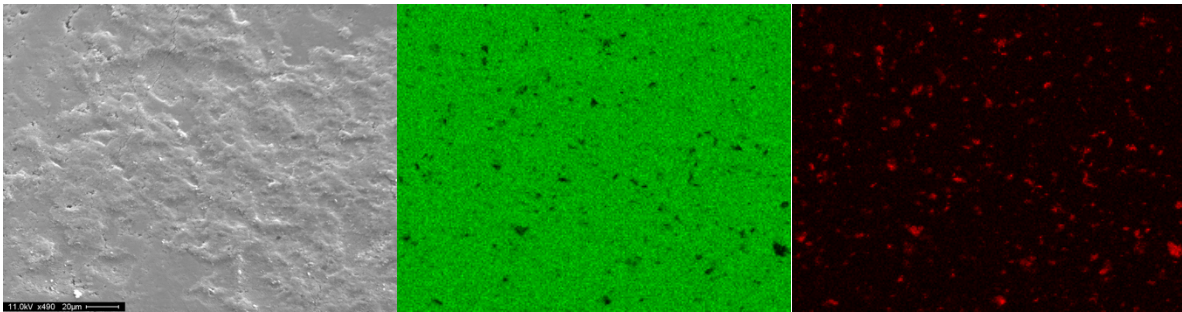


Figure 29 Secondary Electron Microscopy (SEM) Image of 5% InVO₄-TiO₂ (P-25) with Elemental Mapping (EDS) of Ti K in Green and In L in Red (scale bar is 20 μm)

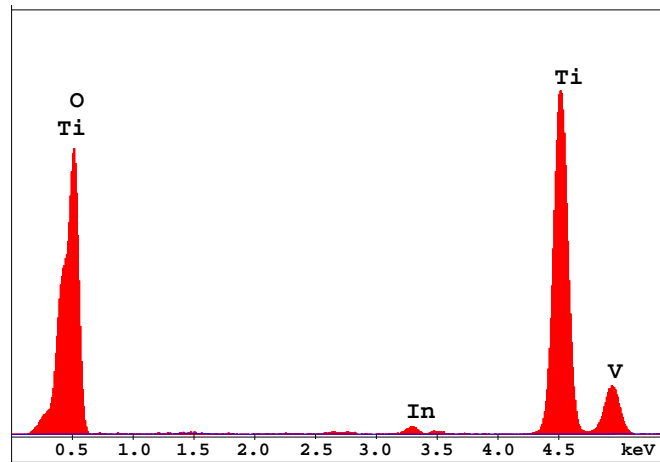


Figure 30 EDS Spectrum of 5% InVO₄-TiO₂ (P-25)

Photocatalytic performance for the degradation of methyl orange was measured over a 3-hour (180 min) period. The normalized concentration curves are shown in Figure 32. Since neither TiO₂ (R) nor 5% InVO₄-TiO₂ (R) demonstrated any conversion, the results were not presented. The greatest degradation was recorded for 2% InVO₄-TiO₂ (P-25) at 91.7%

conversion of methyl orange, which was followed closely by TiO_2 (A) at 91.3% conversion. It is also noted that the 2% $\text{InVO}_4\text{-TiO}_2$ (P-25) yielded higher conversion than the 1, 5 and 10 % $\text{InVO}_4\text{-TiO}_2$ composites. The most striking result was the effect of InVO_4 on anatase TiO_2 . While the addition of InVO_4 on mixed phase titania resulted in a slightly improved degradation (from 85.4% to 91.7% conversion), the addition to anatase resulted in significant retardation of the reaction (from 91.2% to 12.7% conversion). The degradation of methyl orange can be the result of three possible reaction mechanisms: i) oxidation by hydroxyl radicals, ii) oxidation by positively charged holes on the catalyst surface, and iii) reduction by conducting band electrons [11]. Regardless of the mechanisms, the catalytic consequences related to the optimal $\text{InVO}_4\text{:TiO}_2$ (P-25) of 2 % and the activity decrease of 5 % $\text{InVO}_4\text{-TiO}_2$ (A) relative to 5 % TiO_2 (A) indicated the formation of a semiconductor-semiconductor interface. Further investigation of the semiconductor composite is required to elucidate the mechanism of acceleration/retardation.



Figure 31 SEM Micrograph of 5% $\text{InVO}_4\text{-TiO}_2$ (P-25) (scale bar is 1 μm)

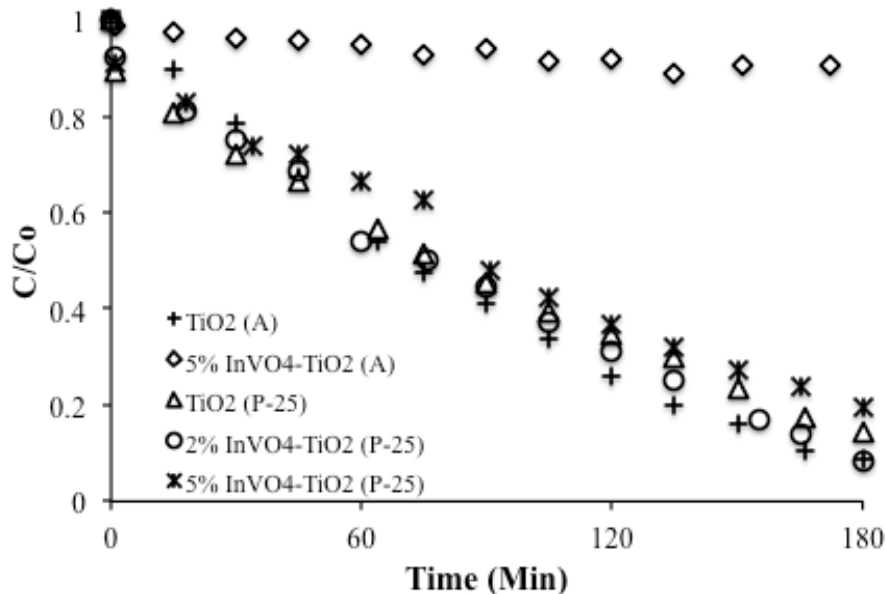


Figure 32 Photocatalytic Degradation of Methyl Orange

3.4 Conclusions

InVO₄-TiO₂ semiconductor composites were made utilizing mixed phase and pure phase titania for photocatalytic degradation of aqueous methyl orange under visible light. A modified complex precursor method followed by calcination was utilized to synthesize orthorhombic indium vanadate powder. This semiconductor powder was then ground via mortar and pestle with titania. Unlike current methods which use sol gels and/or annealing processes that result in anatase phase, this new mechanical method achieved mixed phase titania composites. The addition of InVO₄ to the mixed phase titania resulted in a slightly improved degradation (from 85.4% to 91.7% conversion at t = 3 h) of methyl orange using daylight spectrum radiation. However, the addition to anatase resulted in significant retardation of the reaction (from 91.2% to 12.7% conversion at t = 3 h). Through the avoidance of a calcination step for the composite synthesis, the presented mechanical method achieved single phase and mixed phase titania composites for use as visible range photocatalysts. Moreover, the differences in the catalytic

performance for the InVO₄ addition to single phase and mixed phase titania verified the formation of the semiconductor interface and suggested complex interfacial chemistry.

CHAPTER 4: PHOTOCATALYTIC DEGRADATION OF GEOSMIN AND MIB²

4.1 Introduction

The compounds, 2-methylisoborneol (MIB) and trans-1,10-dimethyl-trans-9-decalol (geosmin), are alicyclic tertiary alcohols produced as secondary metabolites by cyanobacteria and actinomycetes. They are semi-volatiles, which cause musty and earthy flavors and odors in potable water and freshwater fish. They are particularly problematic due to their extremely low threshold for detection by humans, 4 ng/l (ppt) for geosmin and 15 ng/l (ppt) for MIB [51]. Their lipophilic nature results in rapid accumulation in fish tissue, rendering the fillets and roe unpalatable. Harvesting delays and additional processing due to off-flavor compounds have a significant impact on the production cost of cultured freshwater fish. Aquaculture is a growing industry with reported worldwide production in 2010 of \$119 billion, of which approximately 60% were freshwater species [60]. Off-flavor issues are estimated to increase the cost of production of freshwater fish in the United States by 10-20% [84].

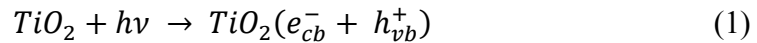
A variety of treatment methods have been explored for the removal of MIB and geosmin. Conventional water treatment methods (coagulation / flocculation / sedimentation / filtration) are ineffective [1, 58]. MIB and geosmin display moderate solubility and moderate hydrophobicity with octanol/ water partition coefficients in the range of 3.1 to 3.7 [56, 58]. Adsorbents such as activated carbon can be effective but may be limited due to the competitive effect of other

² This chapter was submitted to Applied Catalysis B: Environmental (S. Pettit, L. Rodriguez-Gonzalez, J. Michaels, N. Alcantar, S. Ergas, J. Kuhn, *Parameters influencing the photocatalytic degradation of geosmin and 2-methylisoborneol utilizing immobilized TiO₂*, App. Catal. B: Environ.

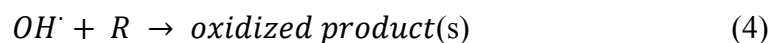
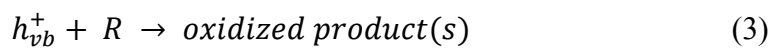
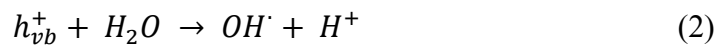
organics in the water, the short life span of the adsorbent, disposal of spent adsorbents, and other operational concerns [56]. Processes that involve phase transfer, like adsorption, have given way to processes that degrade or destroy contaminants. Generally, the most effective treatment methods for taste and odor producing compounds involve oxidation, with advanced oxidation processes (AOPs) having the highest removal rates [1]. AOPs are a class of treatment methods that generate hydroxyl radicals at ambient temperature and atmospheric pressure. They include i) ozone and hydrogen peroxide, ii) UV light and ozone or hydrogen peroxide, and iii) photocatalysis.

Initial studies have shown promising results for TiO₂ photocatalytic reduction of MIB, geosmin, and other persistent aqueous contaminants [10, 39, 55, 85-90]. With the exception of one study utilizing a packed bed of pelletized TiO₂ [90], the noted studies have been conducted in batch slurry systems and are not scalable to aquaculture production facilities due to catalyst separation requirements and operational concerns. Immobilization of the titania photocatalyst would address issues related to separation. However, due to the limited investigations into degradation of these persistent compounds on immobilized titania photocatalysts, additional studies on the parameters and processes that influence degradation are needed.

The activation of TiO₂ can be represented by Eq. (1).

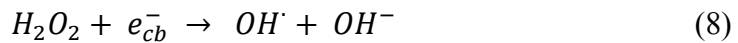
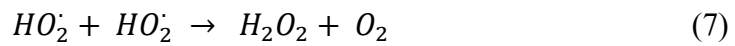


The valence band hole (h_{vb}^+) has a reduction potential of approximately 2.9 V [1], depending on the phase of TiO₂, and can readily oxidize water or organic compounds (R).



Complete oxidation (mineralization) of many organic compounds can be achieved, resulting in carbon dioxide and mineral acid formation [1]. Whether the degradation proceeds via hydroxyl radical attack (Eq. (4)) or direct surface oxidation via the valence band holes (Eq. (3)) has been the subject of debate [11, 16, 89]. Further, some organic molecules can be reduced by the conducting band electrons (e_{cb}^-) to form reactive radical intermediates [11, 89]. A recent study suggested that the predominance of one mechanism over the other is subject to organic compound concentrations, with higher concentrations principally undergoing direct hole oxidation [16].

Several studies have reported the importance of the presence of oxygen for photocatalytic degradation of aqueous organics [6, 40-42, 48, 86, 87]. Oxygen reacts with the conducting band electrons (e_{cb}^-) to form a superoxide radical anion (Eq. (5)). This reaction prevents the accumulation of electrons in the conducting band which if unmitigated would cause an increase in the electron-hole recombination rate. A further contribution rests with the ability of the superoxide radical anion to produce hydroxyl radicals via the following reaction sequence:



Although these contributions are important for the catalytic pathway, oxygen reduction is generally not the rate determining step [87]. Even in studies where increases in rate were observed after addition of bubbled oxygen, the increase was attributed to improved mass transfer along the catalyst surface [40]. Aquaculture systems generally have high levels of dissolved oxygen (DO), which are required to maintain fish health. Water samples from a sturgeon rearing

facility were typically in the range of 9 mg/L DO. The laboratory-prepared geosmin and MIB solutions had significantly lower DO levels. Therefore, the effect of air sparging in the laboratory-prepared samples was investigated in this study.

While a number of treatment methods have shown successful reduction of MIB and geosmin in small-scale laboratory trials, it is important to evaluate operationally scalable systems. In this investigation, we demonstrate the degradation of both MIB and geosmin from naturally tainted water samples utilizing an immobilized TiO₂ photocatalyst. Further, we assess the influence of dissolved oxygen and pH on the degradation rates to optimize process location in an aquaculture production facility. The findings of this work have been incorporated into a larger project, which accesses the continuous operation of TiO₂ photocatalysis in a recirculating aquaculture system (RAS) at MOTE Marine Laboratory Aquaculture Research Park in Sarasota, Florida.

4.2 Experimental

4.2.1 Chemicals and Materials

(-)-Geosmin, 2-methylisoborneol (MIB), and 2-isobutyl-3-methoxypyrazine (IBMP) from Supelco, Sigma-Aldrich were dissolved in analytical grade methanol to prepare stock solutions at concentrations of 1 mg/l (geosmin and MIB) and 100 µg/l (IBMP). Mixed phase titanium dioxide (TiO₂) P-25 was procured from Degussa.

4.2.2 Analytical Method for Geosmin and MIB Quantification

Geosmin and MIB were extracted from aqueous samples using solid-phase microextraction (SPME). The analytical protocol was based upon the 6040 D. Solid-Phase Microextraction method [91]. IBMP, at a final concentration of 10 ng/l, was used as an internal standard. Aliquots (30 ml) were placed in screw-capped 40 ml glass vials with PTFE-faced

silicone septum. Sodium chloride (9 g), IBMP (3 μ l of 100 μ g/l), and a PTFE stir bar were added to the vial which was placed into a 60-65°C water bath. A divinylbenzene/ carboxen/ polydimethylsiloxane (DVB/CAR/PDMS) fiber was extended into the headspace and exposed for 30 min while the sample was magnetically stirred and heated.

After the allotted adsorption time, the SPME fiber was retracted and transferred to the GC-MS injector where the sample was thermally desorbed at 250°C for 3 minutes. Geosmin and MIB were separated using a GC temperature program from 50°C (held for 1 min) to 280°C (held for 1 min) via a ramp rate of 15°C/min. Helium was utilized as the carrier gas (1 ml/min) and for split flow of 50 ml/min, after 2 min of initial splitless operation. The MS was operated in Selective Ion Monitoring (SIM) mode for quantification of analytes. Primary and secondary ions (m/z) for each analyte and internal standard are listed in Table 2. The GC-MS system was comprised of a Perkin Elmer Clarus 580 GC and Clarus 560D MS equipped with a 30 m x 0.25 mm x 0.25 μ m HP-5MS column (Agilent J&W).

Table 2 Ions (m/z) Monitored in SIM Mode GC-MS for Analyte Quantification.

	Primary	Secondary
IBMP	124	151
MIB	95	107, 135
Geosmin	112	126

4.2.3 Experimental Reactor System

The degradation experiments were performed in a laboratory scale reactor system consisting of a glass reservoir (5 L volume), a peristaltic pump (180 ml/min flow), and an aluminum reactor vessel. The vessel was fabricated from reflective aluminum sheet metal with dimensions of 15 in (38.1 cm) long by 2 in (5.1 cm) wide by 1 in (2.5 cm) high. The vessel

cover contained a housing for two 8-watt F8T5 fluorescent bulbs. GE Blacklight Blue bulbs (F8T5BLB) provided irradiance in the UVA spectral range of 350 to 400 nm.

Two 2 in (5.1 cm) x 7 in (20.3 cm) plates of 1/8 in (0.31 cm) borosilicate glass were positioned in the bottom of the reactor vessel. Experimental trials included uncoated plates and plates coated with TiO₂. TiO₂ was utilized as received. The powder catalyst was immobilized onto the glass plates using a slurry spray technique. Based upon desired surface area, catalyst weight was calculated for a target immobilized concentration of 0.25 mg/cm². Using a 1 g catalyst to 20 ml ethanol (95%) ratio, the slurry was mixed using a vibratory plate. Using a Paasche HAPK H#3 airbrush, the slurry was evenly sprayed from a 6 in (15 cm) distance on to the glass substrate. The coated plates were air dried under ambient conditions for 1 h and then calcined in air using a stepped temperature profile from 100° to 500°C for 4 h.

Laboratory trials were performed using distilled water spiked with geosmin and MIB and naturally tainted water collected from a sturgeon rearing RAS facility in Sarasota, Florida. For the primary trials, 2 l of 50 ng/l MIB and 50 ng/l geosmin (which are both similar values to that of the naturally tainted water used in this study and of typical water used at the RAS facility) were added to the reservoir. The fluid was magnetically stirred at 300 rpm and pumped to the reactor vessel at 180 ml/min. The fluid was continuously recirculated through the system and periodically sampled at the reactor outlet. DO and pH were measured from the reservoir using an Orion 5 Star ThermoScientific.

4.3 Results and Discussion

Typical GC-MS chromatograms and spectra are shown in Figures 33 and 34. All analytes eluted as symmetrical peaks within 10 min. The detection limits were 0.8 ng/l for MIB and 0.3 ng/l for geosmin (n=7) with a practical quantification limit of 4 ng/l and 2 ng/l,

respectively. Using the IBMP internal standard, linear calibration relationships were obtained over the range of 0 – 50 ng/l with correlation coefficients of 0.9880 (geosmin) and 0.9842 (MIB).

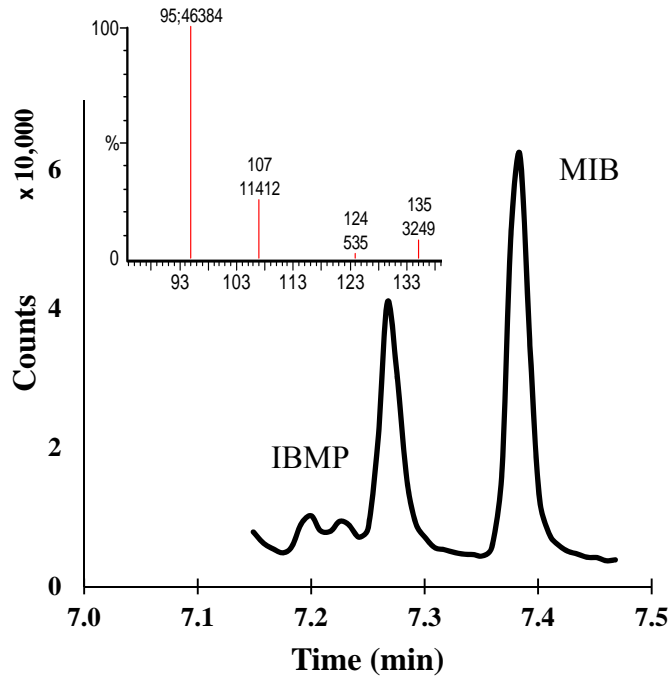


Figure 33 SIM Mode GC Chromatogram Displaying IBMP and MIB with Inset Figure of MIB Mass Spectrum.

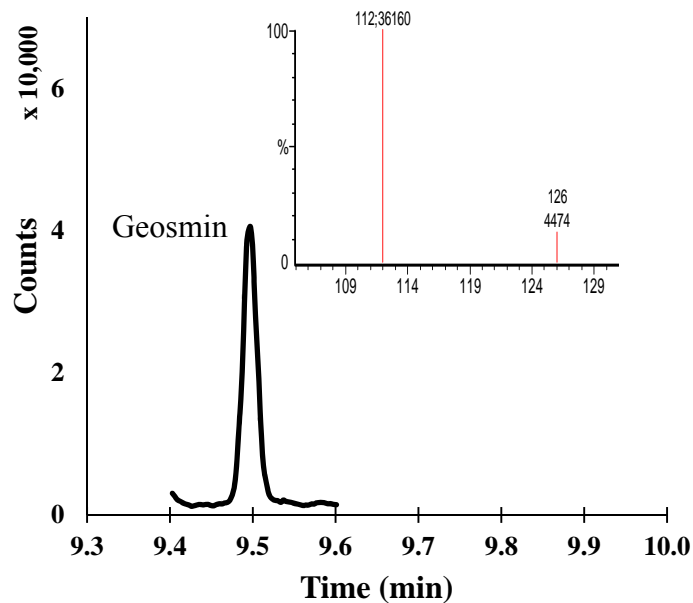


Figure 34 SIM Mode GC Chromatogram Displaying Geosmin with Mass Spectrum Inset Figure.

Initial trials compared the performance of the control (reactor system with uncoated glass plates) to the performance of the immobilized TiO₂. The control system displayed degradation of both geosmin and MIB. This was due to a combination of photolysis, natural degradation, and volatilization due to mixing and a slight temperature increase (up to 3° C over the duration of the trial). Over an 8-hr period, the degradation of MIB and geosmin were 54% and 60% in the TiO₂ photocatalytic system, compared to the control system removal of 48% and 55%, respectively. Although this increase in degradation was relatively small, TiO₂ photocatalysis has been shown by other authors to have additional benefits over the use of photolytic systems. TiO₂ has been shown to effectively degrade or deactivate several strains of toxic microcystins [85, 86, 92] and pathogenic micro-organisms [88]. Microcystin, geosmin, and MIB are all cyanobacteria metabolites and can be found in the same water systems. Further, although UVA treatment inactivated several pathogenic micro-organisms, in prior studies, small variant colonies were observed which could lead to antibiotic resistant infections; these were not observed with TiO₂ photocatalysis [88].

The next series of trials utilized immobilized TiO₂ photocatalyst and examined the effect of oxygen addition via an air sparger in the reservoir tank and the influences of a complex matrix from a naturally tainted water source. As noted previously, the presence of oxygen is necessary for the photocatalytic cycle, but generally not considered a rate determining step. Further, the complex matrix includes a number of hydroxyl radical scavenging species (specifically, carbonate and natural organic matter), which could reduce the degradation rates.

It has been widely reported that degradation of organics via TiO₂ photocatalysis follows Langmuir-Hinshelwood kinetics and at low concentrations can be approximated by pseudo-first order kinetics [6, 11, 38-41]. As shown in Figures 35 and 36, the degradation of geosmin and

pseudo-first order rate constants were determined for the three scenarios: i) 50 ng/l prepared solution, ii) 50 ng/l prepared solution with air sparging, and iii) naturally tainted water. The apparent rate constants for geosmin and MIB are reported in Table 3.

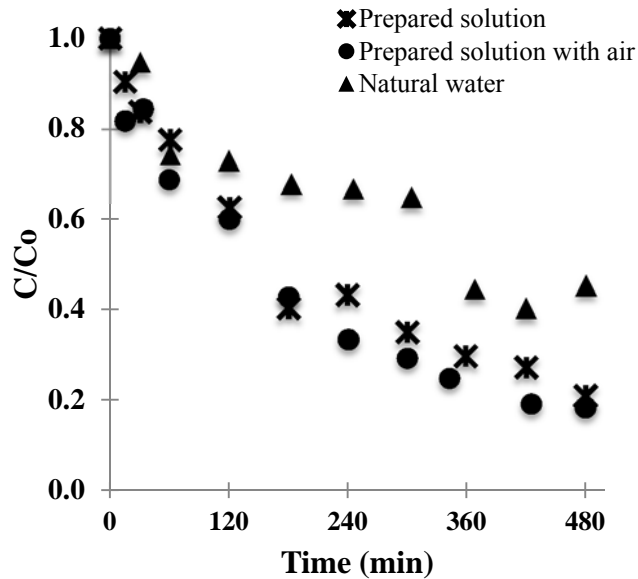


Figure 35 Geosmin Degradation Based on Normalized Concentrations

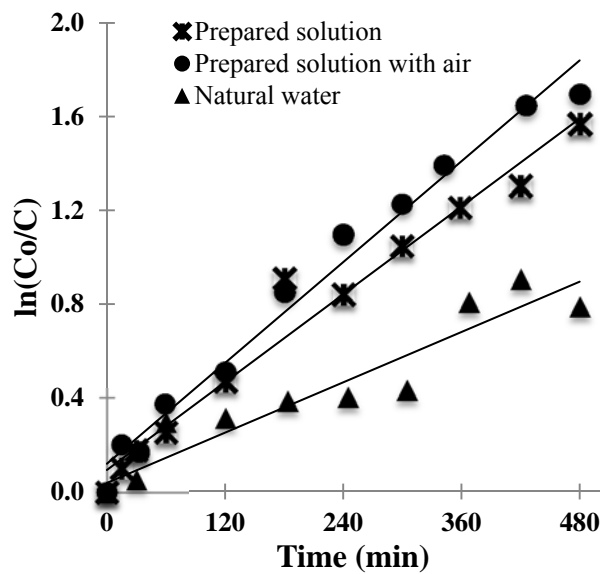


Figure 36 Determination of Pseudo-first Order Rate Constants for Geosmin Degradation

Table 3 Pseudo-first Order Rate Constants (k_{app}) and System Initial pH and Dissolved Oxygen (DO) Content

	MIB k_{app} (10^{-3} min^{-1})	Geosmin k_{app} (10^{-3} min^{-1})	pH	DO (mg/L)
Prepared Solution	2.0	3.1	4.7	7.0
Prepared Solution with air sparging	1.4	3.6	5.3	8.3
Naturally tainted water	1.5	1.7	7.2	9.1

Air sparging in the prepared solutions resulted in a higher rate constant for geosmin and lower rate constant for MIB. To understand this effect, one must also look at the effect of air sparging on the system pH. In systems without air sparging, the pH slowly increased over time, with initial pH values of 4.7 for the prepared solution and 7.2 for the naturally tainted water. With air sparging, the pH fluctuated between 5.3-5.5. Kutschera et al. reported changes to the apparent rate constants of geosmin and MIB at various pH in vacuum UV irradiated systems [59]. Their findings showed that the geosmin rate constant goes through a maxima near a pH of 6 and declines at a greater rate as the system becomes more basic [59]. Further, the MIB rate constant linearly decreases with increasing pH [59]. Our findings for geosmin degradation with TiO_2 photocatalysis correlated well, with the highest rate constant for the air sparged system with a pH of ~ 5.5 . The naturally tainted water scenario had the lowest rate constant, which is expected due to the pH and the addition of other hydroxyl radical scavengers, such as carbonate and natural organic matter.

For MIB, the results for the prepared solutions, with and without air sparging, correlated with the decreasing rate constant with increasing pH. However, in the naturally tainted water

(with a pH of 7-8), a significant decrease in rate constant did not occur, as would have been predicted from the Kutschera et al. findings and the increase in hydroxyl radical scavengers. The explanation for this variance is the surface charge of the immobilized TiO₂. The point of zero charge (pH_{pzc}) for TiO₂ has been reported in the range of 5.8 to 6.25 [6, 41, 93, 94]. Above the pH_{pzc}, the metal oxide surface becomes negatively charged and the oxidation of cationic electron donors and acceptors is favored [41]. It has been reported that one of the degradation intermediates for MIB is the 2-norbornene cation radical [55], which would have preferential oxidation on the catalyst surface at this pH.

Finally, we look at the general trends between MIB and geosmin rate constants. For scenarios with pH values below the pH_{pzc}, geosmin has a significantly higher rate constant than MIB. This would not be predicted from general analysis of the structure. Geosmin with two 6-membered rings has much lower ring strain than MIB with pyramidalized 5-membered rings. The higher ring strain of MIB should translate into enhanced reactivity, but this phenomenon is not observed in the photocatalytic degradation process. Looking at other physical properties, geosmin has a lower aqueous solubility and greater octanol/ water partition coefficient (i.e. greater hydrophobicity), which should drive geosmin towards the catalyst surface. While both geosmin and MIB are degraded by hydroxyl radical attack, the higher degradation rate constants of geosmin could be explained by additional breakdown occurring via direct oxidation on the catalyst surface. This, coupled with the changes in degradation rate constants relative to the point of zero charge, suggested that direct oxidation of organics via the valence band holes plays an important role in the degradation of MIB and geosmin, even at low concentrations. However, regardless of the mechanism, the higher photocatalytic degradation rate constants for geosmin

than MIB is desired because the human detection limit for geosmin is about 4 times lower than MIB.

4.4 Conclusions

The findings of this study demonstrate the successful degradation of MIB and geosmin via an immobilized titania photocatalyst and indicated that the system pH has a significant influence on the degradation rate constants. Geosmin degradation will be maximized near a pH of 6. MIB degradation will be maximized under moderately acidic conditions. However, the effect of increased pH appears to be mediated through the effect of the negative surface charge of the immobilized TiO₂ when the system pH is above the pH_{pzc}. In RAS, nitrification of the wastewater stream consumes alkalinity. Incorporation of the photocatalytic treatment after nitrification and before base addition would maximize MIB and geosmin removal rates.

CHAPTER 5: APPLIED PHOTOCATALYSIS AT MOTE MAP

5.1 System Set-up and Placement

Based upon the findings of the laboratory analysis, a bench scale photocatalytic treatment system was installed at MOTE MAP. Several locations along the existing water treatment train were evaluated for placement of the bench scale system. In addition to pH, natural organic matter (NOM) and carbonate species have a significant impact on the photocatalytic destruction of geosmin and MIB. NOM and carbonate species are hydroxyl radical scavengers, which quench the reaction [1].

Starting the evaluation at the fish culture tank effluent, the high NOM levels make this an ineffective location for the photocatalytic process. After clarifying in the drum filter, the water still has high levels of carbonate. Since oxygen is utilized as an electron acceptor in the photocatalytic process, placement before or after the anaerobic denitrification system poses a compatibility issue. The nitrification system is an aerobic process that consumes alkalinity (i.e. carbonate species). The final compartment oxygenates the water before returning it to the fish culture tanks. Periodically, sodium bicarbonate is added to this compartment to control alkalinity and pH. The placement of the photoreactor must optimize the combination of NOM and carbonate levels, dissolved oxygen (DO), and pH. Typical parameter values are provided in Table 4. Based upon this analysis, the system was located to draw water from the existing water treatment train after nitrification and degassing.

MOTE MAP personnel built a workbench to install a photoreactor on site (Fig. 37). The laboratory flow reactor, as described in Section 2.4.2, was replicated for this application (Fig.

38). The reactor was operated in three eight-hour cycles each day. Each cycle had six continuous hours of UV radiation.

Table 4 Water Analysis

	pH	Alkalinity (mg/L)	DO (mg/L)
Groundwater	7.6	146	7.2
Fish Culture Tank	6.5	94	10.1
Denitrification	6.5	175	2.8
Nitrification	6.6	78	7.3



Figure 37 Placement of Bench Scale Reactor at MOTE MAP



Figure 38 MOTE MAP Bench Scale Reactor System

A five-day continuous operation trial was performed with the MOTE MAP system. Samples were taken from two cycles each day at the end of the 6 h irradiation period. Samples were stored in sealed 40 mL amber vials and refrigerated. At the end of each day, samples were placed in ice in insulated containers and transported to the laboratory for GC-MS analysis.

5.2 Results and Discussion

GC-MS analysis proceeded as previously reported. A number of compounds in addition to geosmin and MIB were present in the water samples collected from MOTE MAP. However,

no significant interference was observed with the elution of IBMP, MIB, or geosmin. The chromatograms are shown in Figures 39 and 40.

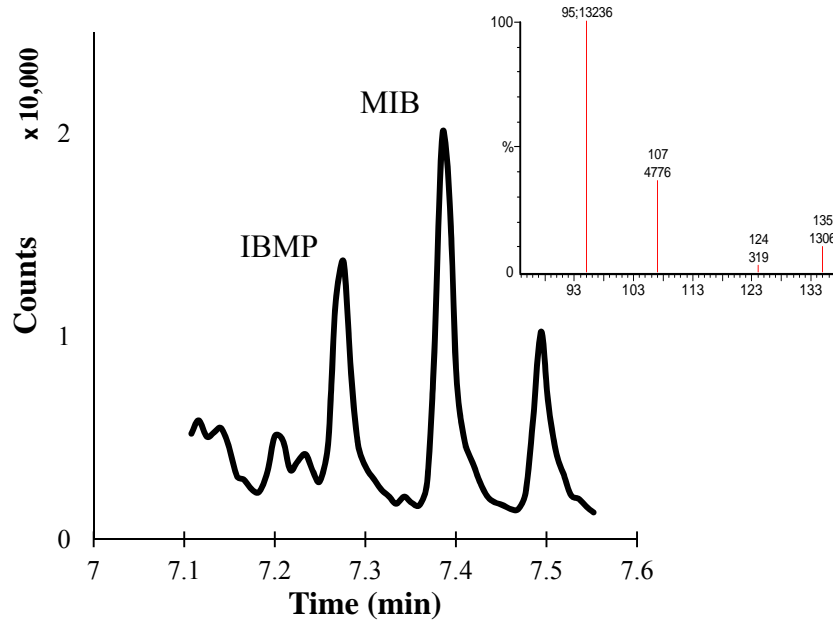


Figure 39 SIM Mode GC Chromatogram Displaying IBMP and MIB with Inset Figure of MIB Mass Spectrum.

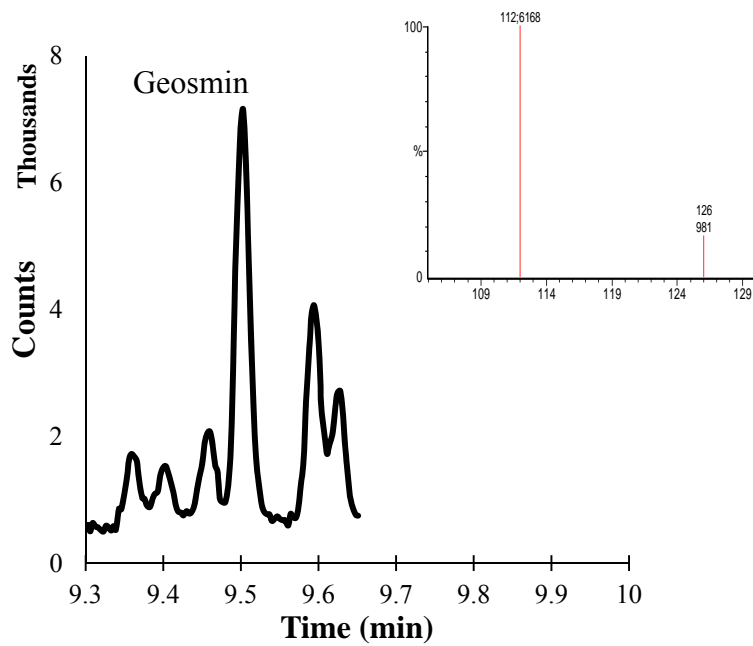


Figure 40 SIM Mode GC Chromatogram Displaying Geosmin with Mass Spectrum Inset Figure.

MIB and geosmin concentrations for the five day trial are reported in Table 5 and compared to the laboratory trial run with MOTE water at the 6 hour point. Generally, the *in situ* trials resulted in higher degradation rates than the laboratory experiment. This can be explained by the difference in pH. The laboratory experiment had an unbuffered pH of 7.2, whereas pH during the trials varied from 6.6 to 6.7. The slightly more acidic conditions improve catalytic performance.

Table 5 MIB and Geosmin Reduction (Concentration in ppt)

		MIB			Geosmin		
		Initial	Treated	Reduction	Initial	Treated	Reduction
Lab		64	27	58%	25	11	56%
<i>In situ</i> trials	1	43	17	62%	36	9	75%
	2	41	13	68%	37	8	78%
	3	43	14	67%	39	9	77%
	4	55	20	64%	37	11	70%
	5	<u>43</u>	<u>19</u>	<u>57%</u>	<u>27</u>	<u>10</u>	<u>63%</u>
Avg		45	16	64%	35	9	73%

To understand the daily variance in reduction, a review of other system parameters is required. Dissolved oxygen averaged 7.2 mg/L with a standard deviation of 0.3. Conductivity averaged 1.4 mS/cm with a standard deviation of 0.3. However, alkalinity varied from 49 to 96 mg/L. Carbonate species (the primary constituents of alkalinity) have a significant impact on photocatalytic efficiency and are the probable cause of the daily variance in MIB and geosmin reduction.

Alkalinity is a dynamic parameter in aquaculture systems. In the denitrification reactor, a carbon source (eg. molasses) is oxidized into CO₂ and alkalinity is increased. During nitrification, carbonate species are consumed during the conversion of ammonia into nitrite and

nitrate. The net effect of the combined processes is the reduction of alkalinity. For a continuous operation, sodium bicarbonate is added to the system to balance the net loss from the nitrification /denitrification process. Addition of excess molasses or sodium bicarbonate can cause an imbalance in the carbonate levels. Further, pH and temperature can affect the metabolic rates of the bacteria, also leading to a carbonate imbalance.

Ideally, reduction of geosmin and MIB would result in concentrations below the human detection threshold (4 ppt for geosmin and 15 ppt for MIB). The system as currently designed nearly reaches this goal at 9 ppt and 16 ppt, respectively.

CHAPTER 6: CONCLUSIONS AND FUTURE WORK

6.1 Conclusions

As presented in Chapter 1, the *specific goals* of this work included:

1. Development of a novel synthesis method, which allows the independent variance of dopant material and titania crystal phase.
2. Elucidation of the correlation between crystalline phase and dopant effects.
3. Demonstration of the reduction of target, trace level concentration contaminants in a complex water matrix.

Relative to the first goal, Chapter 3 presented a novel synthesis method for the creation of semiconductor composites using InVO_4 and TiO_2 . This method is envisioned to be a platform for the synthesis of other composite catalysts. It affords moderate tailoring of the dopant and crystal phase ratio parameters.

Using InVO_4 - TiO_2 composites of varying titania crystallinity, the degradation of methyl orange and 2-chlorophenol were observed. The dopant enhancement (or retardation) was dependent upon crystal phase and the reaction under consideration. Further work is recommended to confirm hypotheses associated with this correlation.

Finally, Chapters 4 and 5 demonstrated the laboratory and *in situ* degradation of MIB and geosmin from recirculating aquaculture systems. Chapter 4 documented the ability to immobilize TiO_2 for the treatment of flowing streams. Moreover, the effect of key parameters, including pH and dissolved oxygen, on the degradation of geosmin and MIB were analyzed. Chapter 5 detailed the efficacy of this system applied in a recirculating aquaculture system.

Ultimately, catalyst photoinitiation by solar radiation would be desirable and preliminary investigation is presented in the proposed future work below.

6.2 Future Work

6.2.1 Pure and Mixed Phase Titania

The visible light photocatalytic degradation of methyl orange was analyzed for composites with varying TiO₂ crystallinity. While modest improvements to methyl orange degradation were seen with the mixed phase composite, the degradation of 2-chlorophenol showed significant enhancement.

An unexpected result of this work was the retardation of the methyl orange degradation rate when InVO₄ was added to anatase TiO₂. It has been suggested that methyl orange degradation can proceed via direct reduction by surface electrons (e_{cb}^-), as well as oxidation by hydroxyl radicals or surface holes (h_{vb}^+) [11]. InVO₄ is an n-type semiconductor [79] that may transport electrons away from the titania surface. If methyl orange degradation occurs via direct reduction by the surface electron, doping with InVO₄ would retard the degradation. This theory could be tested by introduction of another electron scavenger (e.g. dissolved oxygen) at high concentrations into the system.

6.2.2 Visible Light Photoinitiation for MIB and Geosmin Reduction

Feasibility of an immobilized InVO₄-TiO₂ composite was examined for the visible light initiated photodegradation of geosmin and MIB. Initial trials indicate that the visible light initiated composite has similar degradation rates to the UV initiated TiO₂ process (Fig. 41) for distilled water samples spiked with geosmin and MIB.

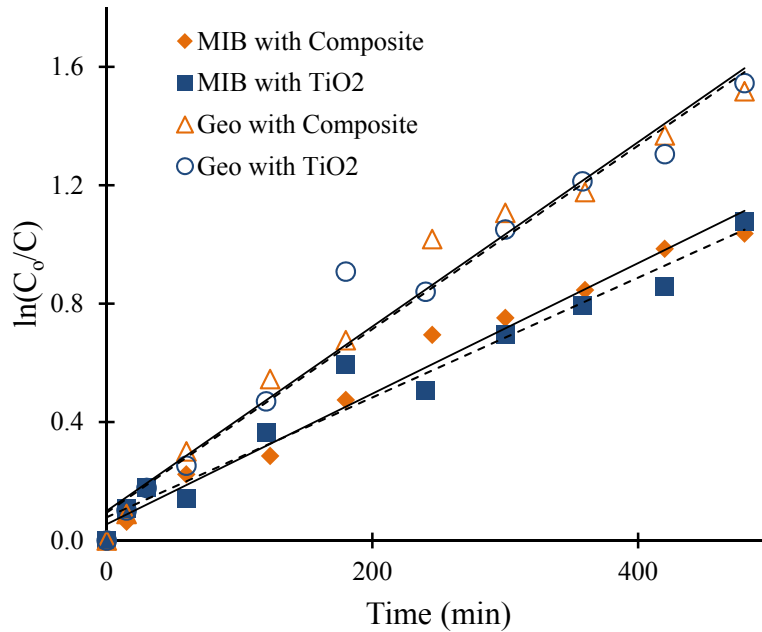


Figure 41 Comparison of UV Initiated TiO₂ and Visible Light Initiated TiO₂-InVO₄ Composite for the Photocatalytic Degradation of Geosmin and MIB

Repetition of the trials with naturally tainted water is suggested with visible light and the InVO₄-TiO₂ composite. The pH_{pzc} of the composite is 5.8 (as determined by KAU). Although this is at the lower limit of the typical range for TiO₂, the interfacial chemistry between the two semiconductors may affect analyte adsorption and reaction sites.

REFERENCES

- [1] J. Crittenden, R. Trussell, D. Hand, K. Howe, G. Tchobanoglous, H. Montgomery Watson, *Water treatment : principles and design / MWH, Inc. ; revised by John C. Crittenden ... [et al.]*, 2nd ed. ed., J. Wiley, Hoboken, N.J, 2005.
- [2] G.L. Li, Z. Yin, *PCCP* 13 (2011) 2824-2833.
- [3] B. Ohtani, O.O. Prieto-Mahaney, D. Li, R. Abe, *Journal of Photochemistry and Photobiology A: Chemistry* 216 (2010) 179-182.
- [4] K.E. Rajashekhar, L.G. Devi, *J. Mol. Catal. A: Chem.* 374–375 (2013) 12-21.
- [5] W. Choi, A. Termin, M.R. Hoffmann, *J. Phys. Chem.* 98 (1994) 13669-13679.
- [6] S. Ahmed, M.G. Rasul, W.N. Martens, R. Brown, M.A. Hashib, *Desalination* 261 (2010) 3-18.
- [7] Q. Sun, Y. Xu, *J. Phys. Chem. C* 114 (2010) 18911-18918.
- [8] M. Dhayal, S.D. Sharma, C. Kant, K.K. Saini, S.C. Jain, *Surf. Sci.* 602 (2008) 1149-1154.
- [9] M.B. Fisher, D.A. Keane, P. Fernández-Ibáñez, J. Colreavy, S.J. Hinder, K.G. McGuigan, S.C. Pillai, *Applied Catalysis B: Environmental* 130–131 (2013) 8-13.
- [10] B. Gao, P.S. Yap, T.M. Lim, T.-T. Lim, *Chem. Eng. J.* 171 (2011) 1098-1107.
- [11] N. Guettaï, H. Ait Amar, *Desalination* 185 (2005) 427-437.
- [12] J. Liu, Y. Yu, Z. Liu, S. Zuo, B. Li, *Int. J. Photoenergy* 2012 (2012).
- [13] T. Ohno, M. Akiyoshi, T. Umebayashi, K. Asai, T. Mitsui, M. Matsumura, *Appl. Catal., A* 265 (2004) 115-121.
- [14] R. Rattanakam, S. Supothina, *Res. Chem. Intermed.* (2009) 263.
- [15] R. Su, R. Bechstein, L. Sør, R.T. Vang, M. Sillassen, B. Esbjörnsson, A. Palmqvist, F. Besenbacher, *J. Phys. Chem. C* 115 (2011) 24287-24292.
- [16] L. Yu, J. Xi, M.-D. Li, H.T. Chan, T. Su, D.L. Phillips, W.K. Chan, *PCCP* 14 (2012) 3589-3595.

- [17] C. Shifu, C. Lei, G. Shen, C. Gengyu, *Powder Technol.* 160 (2005) 198-202.
- [18] R. Daghrir, P. Drogui, D. Robert, *Industrial & Engineering Chemistry Research* 52 (2013) 3581-3599.
- [19] A. Sclafani, J.M. Herrmann, *The Journal of Physical Chemistry* 100 (1996) 13655-13661.
- [20] M.A. Henderson, *Surf. Sci. Rep.* 66 (2011) 185-297.
- [21] A.G. Agrios, K.A. Gray, E. Weitz, *Langmuir* 19 (2003) 1402-1409.
- [22] D. Gummy, S.A. Giraldo, J. Rengifo, C. Pulgarin, *Applied Catalysis B: Environmental* 78 (2008) 19-29.
- [23] T. Ohno, K. Sarukawa, K. Tokieda, M. Matsumura, *J. Catal.* 203 (2001) 82-86.
- [24] D.C. Hurum, A.G. Agrios, K.A. Gray, T. Rajh, M.C. Thurnauer, *J. Phys. Chem. B* 107 (2003) 4545-4549.
- [25] G. Li, C.P. Richter, R.L. Milot, L. Cai, C.A. Schmuttenmaer, R.H. Crabtree, G.W. Brudvig, V.S. Batista, *Dalton Transactions* (2009) 10078-10085.
- [26] Y.K. Kho, A. Iwase, W.Y. Teoh, L. Mädler, A. Kudo, R. Amal, *The Journal of Physical Chemistry C* 114 (2010) 2821-2829.
- [27] C.-M. Huang, L.-C. Chen, K.-W. Cheng, G.-T. Pan, *J. Mol. Catal. A: Chem.* 261 (2007) 218-224.
- [28] R. Nakamura, T. Tanaka, Y. Nakato, *J. Phys. Chem. B* 108 (2004) 10617-10620.
- [29] Y. Wang, C. Feng, Z. Jin, J. Zhang, J. Yang, S. Zhang, *J. Mol. Catal. A: Chem.* 260 (2006) 1-3.
- [30] S. Sakthivel, H. Kisch, *Angew. Chem. Int. Ed.* 42 (2003) 4908-4911.
- [31] N. Feng, Q. Wang, A. Zheng, Z. Zhang, J. Fan, S.-B. Liu, J.-P. Amoureux, F. Deng, *J. Am. Chem. Soc.* 135 (2013) 1607-1616.
- [32] S.A.K. Leghari, S. Sajjad, F. Chen, J. Zhang, *Chem. Eng. J.* 166 (2011) 906-915.
- [33] S. Coste, G. Bertrand, C. Coddet, E. Gaffet, H. Hahn, H. Sieger, *J. Alloys Compd.* 434-435 (2007) 489-492.
- [34] S. Bégin-Colin, T. Girot, G. Le Caër, A. Mocellin, *J. Solid State Chem.* 149 (2000) 41-48.
- [35] T. Girot, S. Bégin-Colin, X. Devaux, G. Le Caër, A. Mocellin, *J. Mater. Synth. Process.* 8 (2000) 139-144.

- [36] L. Ge, M. Xu, H. Fang, *Mater. Lett.* 61 (2007) 63-66.
- [37] L. Ge, M.X. Xu, M. Sun, *Mater. Lett.* 60 (2006) 287-290.
- [38] L. Andronic, A. Duta, *Mater. Chem. Phys.* 112 (2008) 1078-1082.
- [39] L.A. Lawton, P.K.J. Robertson, R.F. Robertson, F.G. Bruce, *Applied Catalysis B: Environmental* 44 (2003) 9-13.
- [40] M.F.J. Dijkstra, A. Michorius, H. Buwalda, H.J. Panneman, J.G.M. Winkelman, A.A.C.M. Beenackers, *Catal. Today* 66 (2001) 487-494.
- [41] M.R. Hoffmann, S.T. Martin, W. Choi, D.W. Bahnemann, *Chem. Rev.* 95 (1995) 69-96.
- [42] A.L. Linsebigler, G. Lu, J. John T Yates, *Chem. Rev.* 95 (1995) 735-758.
- [43] A. Bouzoubaa, A. Markovits, M. Calatayud, C. Minot, *Surf. Sci.* 583 (2005) 107-117.
- [44] L. Kavan, M. Grätzel, S.E. Gilbert, C. Klemenz, H.J. Scheel, *J. Am. Chem. Soc.* 118 (1996) 6716-6723.
- [45] D.O. Scanlon, C.W. Dunnill, J. Buckeridge, S.A. Shevlin, A.J. Logsdail, S.M. Woodley, C.R.A. Catlow, M.J. Powell, R.G. Palgrave, I.P. Parkin, G.W. Watson, T.W. Keal, P. Sherwood, A. Walsh, A.A. Sokol, *Nat Mater* 12 (2013) 798-801.
- [46] N. Guettaï, H. Ait Amar, *Desalination* 185 (2005) 439-448.
- [47] L. Ge, M. Xu, H. Fang, *Appl. Surf. Sci.* 253 (2006) 2257-2263.
- [48] L. Ge, M. Xu, H. Fang, *J. Mol. Catal. A: Chem.* 258 (2006) 68-76.
- [49] Z. Ping, X. Mingxia, F. Haibo, L. Lingxia, *Mater. Lett.* 63 (2009) 2146-2148.
- [50] M. Huang, C. Xu, Z. Wu, Y. Huang, J. Lin, J. Wu, *Dyes and Pigments* 77 (2008) 327-334.
- [51] W.F. Young, H. Horth, R. Crane, T. Ogden, M. Arnott, *Water Res.* 30 (1996) 331-340.
- [52] M. Drikas, M. Dixon, J. Morran, *Water Res.* 43 (2009) 5151-5159.
- [53] D. Cook, G. Newcombe, P. Sztajn bok, *Water Res.* 35 (2001) 1325-1333.
- [54] J. Ellis, W. Korth, *Water Res.* 27 (1993) 535-539.
- [55] S.-J. Yoon, Y.H. Lee, W.-J. Cho, I.-O. Koh, M. Yoon, *Catal. Commun.* 8 (2007) 1851-1856.
- [56] L. Guttman, J. van Rijn, *Aquaculture* 279 (2008) 85-91.

- [57] R. Srinivasan, G.A. Sorial, *Journal of Environmental Sciences* 23 (2011) 1-13.
- [58] W. Song, K.E. O'Shea, *Water Res.* 41 (2007) 2672-2678.
- [59] K. Kutschera, H. Börnick, E. Worch, *Water Res.* 43 (2009) 2224-2232.
- [60] A.M. Mathiesen, *The State of World Fisheries and Aquaculture 2012*, in: F.a.A. Department (Ed.), *Food and Agriculture Organization of the United Nations*, Rome, 2012.
- [61] K. Knickerbocker, *Florida Aquaculture Plan Fiscal Year 2014-2015*, in: D.o.A.a.C. Services (Ed.), 10/2013 ed., State of Florida, Tallahassee, 2013.
- [62] L. Zhang, H. Fu, C. Zhang, Y. Zhu, *J. Solid State Chem.* 179 (2006) 804-811.
- [63] B. Orel, A. Surca Vuk, U. Opara Krasovec, G. Drazic, *Electrochim. Acta* 46 (2001) 2059-2068.
- [64] L. Ge, M. Xu, *Mater. Sci. Eng., B* 131 (2006) 222-229.
- [65] G. Li, Y. Tian, P. Zhang, *J. Sol-Gel Sci. Technol.* 52 (2009) 15-18.
- [66] H.-Y. Lin, Y.-F. Chen, Y.-W. Chen, *Int. J. Hydrogen Energy* 32 (2007) 86-92.
- [67] Y. Min, K. Zhang, Y. Chen, Y. Zhang, *Ultrason. Sonochem.* 19 (2012) 883-889.
- [68] S. Pettit, C. McCane, J. Wolan, J. Kuhn, *Catal. Lett.* 143 (2013) 772-776.
- [69] J. Ye, Z. Zou, M. Oshikiri, A. Matsushita, M. Shimoda, M. Imai, T. Shishido, *Chem. Phys. Lett.* 356 (2002) 221-226.
- [70] C.K. Lee, D.K. Kim, J.H. Lee, J.H. Sung, I. Kim, K.H. Lee, J.W. Park, Y.K. Lee, *J. Sol-Gel Sci. Technol.* 31 (2004) 67-72.
- [71] H.-J. Hübschmann, *Handbook of GC/MS : fundamentals and applications / Hans-Joachim Hübschmann*, Weinheim : Chichester : Wiley-VCH, c2001., 2001.
- [72] P.B. Johnsen, J.-C.W. Kuan, *J. Chromatogr. A* 409 (1987) 337-342.
- [73] B. Hurlburt, S.W. Lloyd, C.C. Grimm, *J. Chromatogr. Sci.* 47 (2009) 670-673.
- [74] S.B. Watson, B. Brownlee, T. Satchwill, E.E. Hargesheimer, *Water Res.* 34 (2000) 2818-2828.
- [75] K. Saito, K. Okamura, H. Kataoka, *J. Chromatogr. A* 1186 (2008) 434-437.
- [76] *AWWA Manual of Water Supply Practices: M57, Algae: Source to Treatment*, 2010 ed., American Water Works Association, 2010.

- [77] W. Yao, B. Zhang, C. Huang, C. Ma, X. Song, Q. Xu, *J. Mater. Chem.* 22 (2012) 4050-4055.
- [78] L. Chen, Y. Liu, Z. Lu, D. Zeng, *J. Colloid Interface Sci.* 295 (2006) 440-444.
- [79] C.S. Enache, D. Lloyd, M.R. Damen, J. Schoonman, R.V. de Krol, *J. Phys. Chem. C* 113 (2009) 19351-19360.
- [80] S. Denis, E. Baudrin, M. Touboul, J.-M. Tarascon, *J. Electrochem. Soc.* 144 (1997) 4099-4109.
- [81] M. Touboul, K. Melghit, P. Benard, *Eur. J. Solid State Inorg. Chem.* 31 (1994) 151-161.
- [82] M. Touboul, K. Melghit, P. Bénard, D. Louër, *J. Solid State Chem.* 118 (1995) 93-98.
- [83] S. Zhang, C. Zhang, H. Yang, Y. Zhu, *J. Solid State Chem.* 179 (2006) 873-882.
- [84] K.K. Schrader, M.Q. de Regt, P.D. Tidwell, C.S. Tucker, S.O. Duke, *Aquaculture* 163 (1998) 85-99.
- [85] L.A. Lawton, P.K.J. Robertson, B.J.P.A. Cornish, I.L. Marr, M. Jaspars, *J. Catal.* 213 (2003) 109-113.
- [86] P.K.J. Robertson, L.A. Lawton, B.J.P.A. Cornish, M. Jaspars, *Journal of Photochemistry and Photobiology A: Chemistry* 116 (1998) 215-219.
- [87] P.K.J. Robertson, D.W. Bahnemann, L.A. Lawton, E. Bellu, *Applied Catalysis B: Environmental* 108-109 (2011) 1-5.
- [88] J.M.C. Robertson, P.K. J. Robertson, L.A. Lawton, *Journal of Photochemistry and Photobiology A: Chemistry* 175 (2005) 51-56.
- [89] A. Oliveira, E.M. Saggiaro, T. Pavesi, J.C. Moreira, L.F.V. Ferreira, in: S. Saha (Ed.), *Molecular Photochemistry - Various Aspects*, Intech, <http://www.intechopen.com>, 2012.
- [90] C.J. Pestana, P.K.J. Robertson, C. Edwards, W. Wilhelm, C. McKenzie, L.A. Lawton, *Chem. Eng. J.* 235 (2014) 293-298.
- [91] E.W. Rice, R.B. Baird, A.D. Eaton, L.S. Clesceri, *Standard methods for the examination of water & wastewater* 22nd edition, Washington, DC : American Public Health Association, c2012. 22nd ed. / prepared and published jointly by American Public Health Association, American Water Works Association, Water Environment Federation ; joint editorial board, Eugene W. Rice ... [et al.] ; managing editor, Laura Bridgewater., 2012.
- [92] M.G. Antoniou, J.A. Shoemaker, A.A. de la Cruz, D.D. Dionysiou, *Toxicon* 51 (2008) 1103-1118.
- [93] C.E. McNamee, Y. Tsujii, M. Matsumoto, *Langmuir* 21 (2005) 11283-11288.

- [94] M. Kosmulski, Chemical properties of material surfaces / Marek Kosmulski, New York : Marcel Dekker, c2001., 2001.

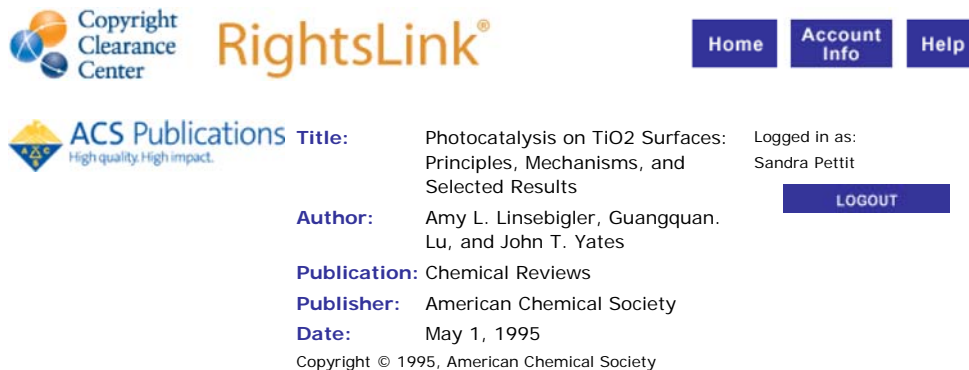
APPENDICES

Appendix A Copyright Permissions

A.1 Permission for Use of Material in Figure 1

Rightslink® by Copyright Clearance Center

https://s100.copyright.com/AppDispatchServlet#formTop



The screenshot shows the RightsLink interface. At the top left is the Copyright Clearance Center logo. To its right is the RightsLink logo. Further right are three navigation buttons: Home, Account Info, and Help. Below the logos is the ACS Publications logo with the tagline "High quality. High impact." To the right of the ACS logo, the following information is displayed:

Title: Photocatalysis on TiO₂ Surfaces: Principles, Mechanisms, and Selected Results
Author: Amy L. Linsebigler, Guangquan Lu, and John T. Yates
Publication: Chemical Reviews
Publisher: American Chemical Society
Date: May 1, 1995

Logged in as: Sandra Pettit
[LOGOUT](#)

Copyright © 1995, American Chemical Society

PERMISSION/LICENSE IS GRANTED FOR YOUR ORDER AT NO CHARGE

This type of permission/license, instead of the standard Terms & Conditions, is sent to you because no fee is being charged for your order. Please note the following:

- Permission is granted for your request in both print and electronic formats, and translations.
- If figures and/or tables were requested, they may be adapted or used in part.
- Please print this page for your records and send a copy of it to your publisher/graduate school.
- Appropriate credit for the requested material should be given as follows: "Reprinted (adapted) with permission from (COMPLETE REFERENCE CITATION). Copyright (YEAR) American Chemical Society." Insert appropriate information in place of the capitalized words.
- One-time permission is granted only for the use specified in your request. No additional uses are granted (such as derivative works or other editions). For any other uses, please submit a new request.

If credit is given to another source for the material you requested, permission must be obtained from that source.

A.2 Permission for Use of Material in Figure 2

Rightslink® by Copyright Clearance Center

https://s100.copyright.com/AppDispatchServlet

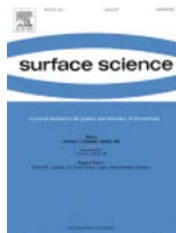


RightsLink®

Home

Account Info

Help



Title: Comparison of the reduction of metal oxide surfaces: TiO₂-anatase, TiO₂-rutile and SnO₂-rutile

Author: Asmae Bouzoubaa, Alexis Markovits, Mònica Calatayud, Christian Minot

Publication: Surface Science

Publisher: Elsevier

Date: 20 May 2005

Copyright © 2005, Elsevier

Logged in as:

Sandra Pettit

Account #:

3000737538

LOGOUT

Order Completed

Thank you very much for your order.

This is a License Agreement between Sandra Pettit ("You") and Elsevier ("Elsevier"). The license consists of your order details, the terms and conditions provided by Elsevier, and the [payment terms and conditions](#).

[Get the printable license.](#)

License Number	3305110505622
License date	Jan 09, 2014
Licensed content publisher	Elsevier
Licensed content publication	Surface Science
Licensed content title	Comparison of the reduction of metal oxide surfaces: TiO ₂ -anatase, TiO ₂ -rutile and SnO ₂ -rutile
Licensed content author	Asmae Bouzoubaa, Alexis Markovits, Mònica Calatayud, Christian Minot
Licensed content date	20 May 2005
Licensed content volume number	583
Licensed content issue number	1
Number of pages	11
Type of Use	reuse in a thesis/dissertation
Portion	figures/tables/illustrations
Number of figures/tables /illustrations	1
Format	both print and electronic
Are you the author of this Elsevier article?	No
Will you be translating?	No
Title of your thesis/dissertation	Investigation of TiO ₂ and InVO ₄ -TiO ₂ semiconductors for photocatalytic degradation of aqueous organics
Expected completion date	Mar 2014

A.3 Permission for Use of Material in Chapter 3

Rightslink® by Copyright Clearance Center

https://s100.copyright.com/AppDispatchServlet



RightsLink®

Home

Account Info

Help



Title: Synthesis, Characterization, and Photocatalytic Degradation Performances of Composite Photocatalytic Semiconductors (InVO4–TiO2) Using Pure and Mixed Phase Titania Powders

Logged in as:
Sandra Pettit

LOGOUT

Author: Sandra L. Pettit

Publication: Catalysis Letters

Publisher: Springer

Date: Jan 1, 2013

Copyright © 2013, Springer Science+Business Media
New York

Order Completed

Thank you very much for your order.

This is a License Agreement between Sandra Pettit ("You") and Springer ("Springer"). The license consists of your order details, the terms and conditions provided by Springer, and the [payment terms and conditions](#).

[Get the printable license.](#)

License Number	3305000823495
License date	Jan 09, 2014
Licensed content publisher	Springer
Licensed content publication	Catalysis Letters
Licensed content title	Synthesis, Characterization, and Photocatalytic Degradation Performances of Composite Photocatalytic Semiconductors (InVO4–TiO2) Using Pure and Mixed Phase Titania Powders
Licensed content author	Sandra L. Pettit
Licensed content date	Jan 1, 2013
Volume number	143
Issue number	8
Type of Use	Thesis/Dissertation
Portion	Full text
Number of copies	1
Author of this Springer article	Yes and you are the sole author of the new work
Title of your thesis / dissertation	Investigation of TiO2 and InVO4-TiO2 semiconductors for photocatalytic degradation of aqueous organics
Expected completion date	Mar 2014
Estimated size(pages)	100
Total	0.00 USD

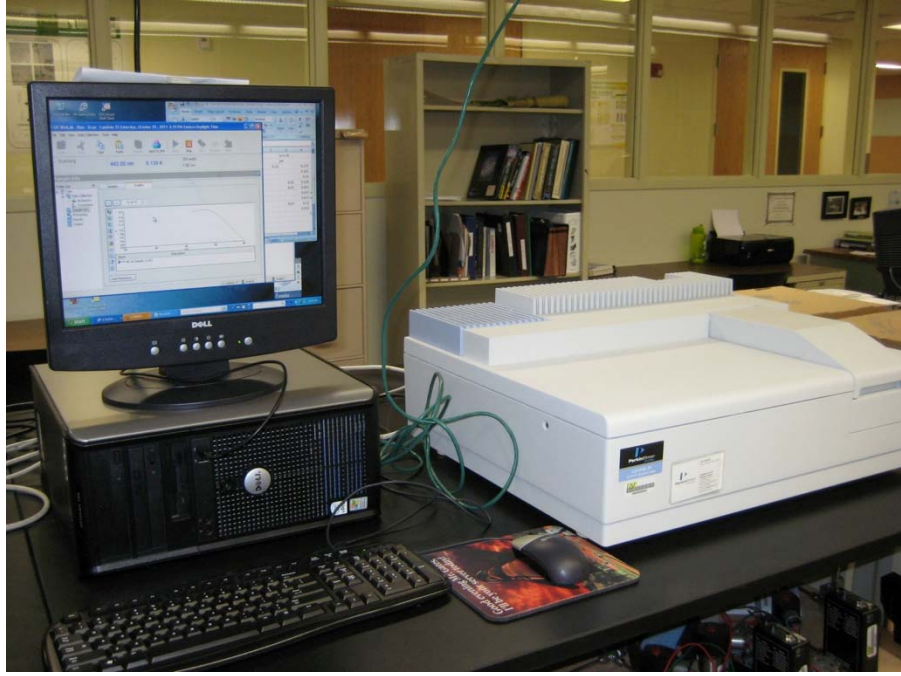
Appendix B Instrumentation



Figure B-1 Bio Rad Excalibur FTS 3000 FTIR – External and Internal Views



Figure B-2 PIKE ATR Sample Holder



(a)



(b)

Figure B-3 Perkin Elmer Lambda 35 UV-Vis Spectrometer (a) with Dual Beam Detection (b)



Figure B-4 Eppendorf Centrifuge



Figure B-5 Perkin Elmer Clarus GC-MS

Appendix C Supplemental Data

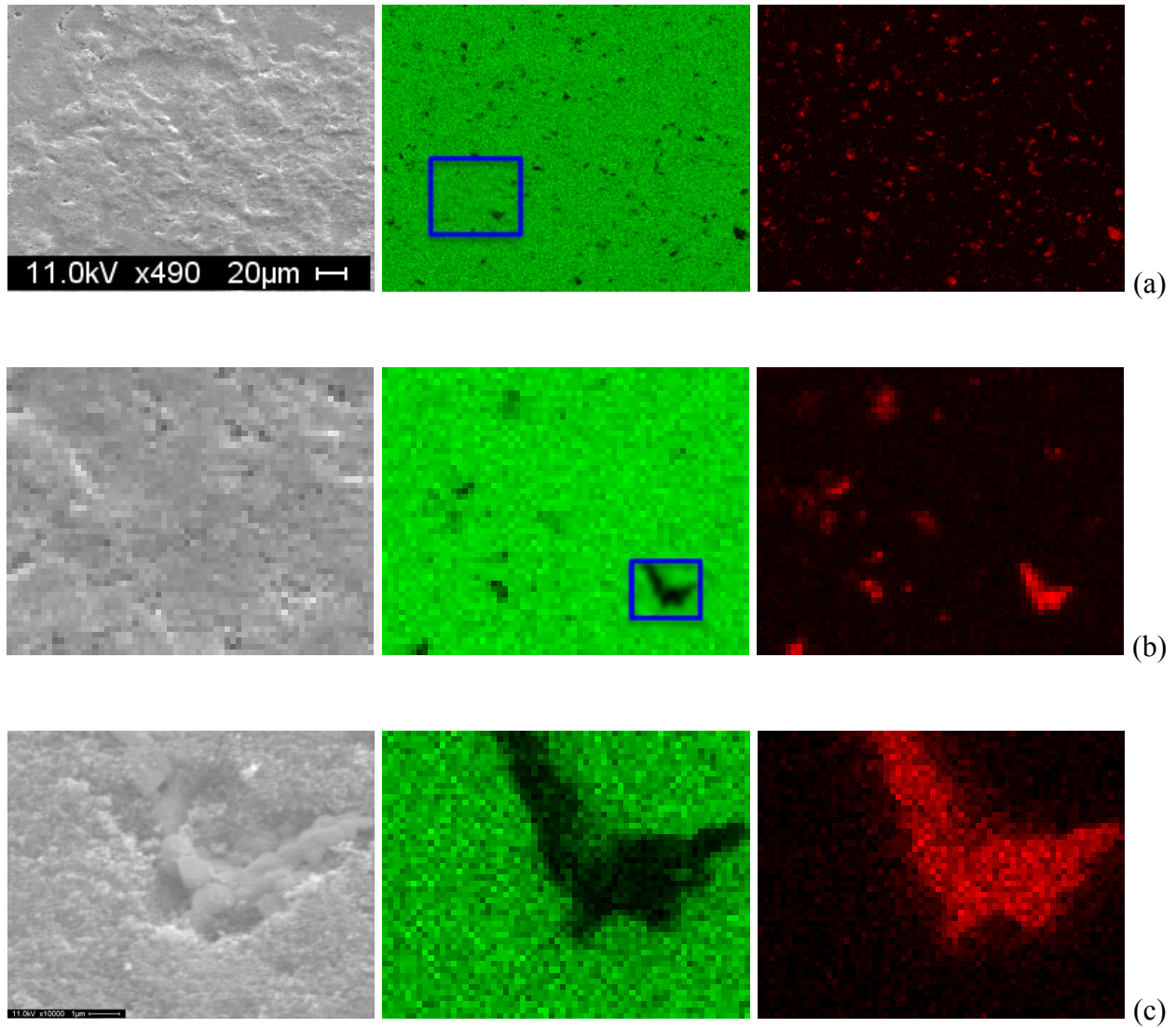


Figure C-1 5% InVO₄-TiO₂ SEM Images and EDS Elemental Maps with Progressive Magnification. Ti K α emission (center) is mapped in green and In L α emission (right) in red. Magnification increases from 490 in (a) series to 2000 in (b) series to 10,000 in (c) series. Scale bar in (c) series is 1 μ m.

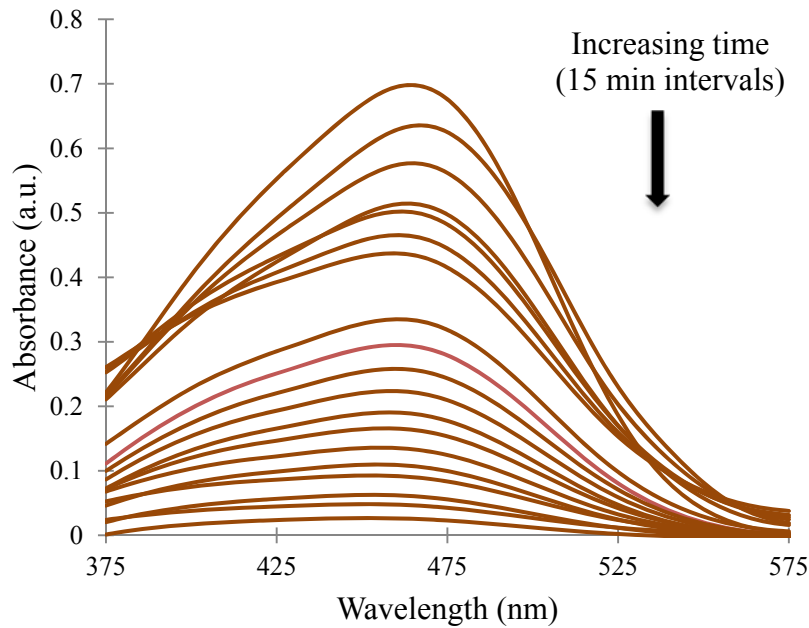


Figure C-2 Typical Time Lapsed Methyl Orange Absorbance. Aliquots were taken every 15 min from slurry solution containing 5% $\text{InVO}_4\text{-TiO}_2$ (P-25).

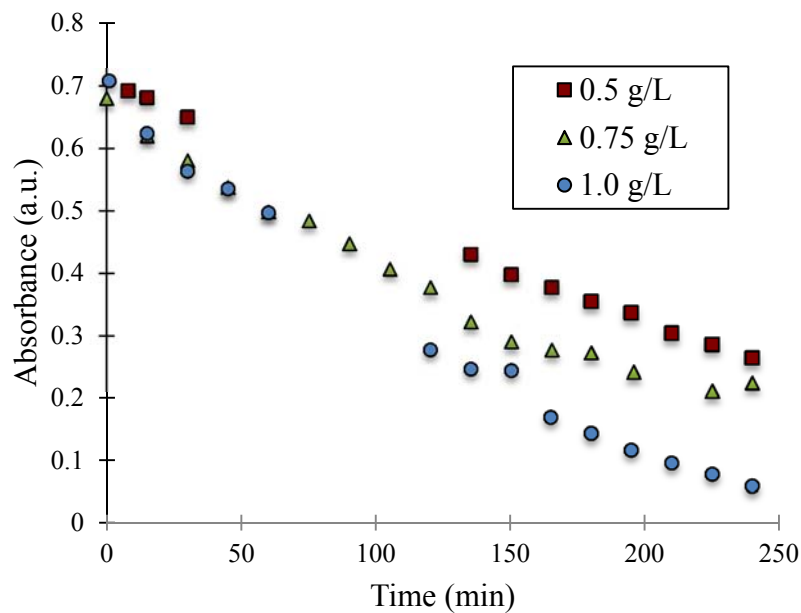


Figure C-3 Effect of Catalyst Dosing Rate on Methyl Orange Degradation. Dosing study performed with 5% $\text{InVO}_4\text{-TiO}_2$ (P-25).

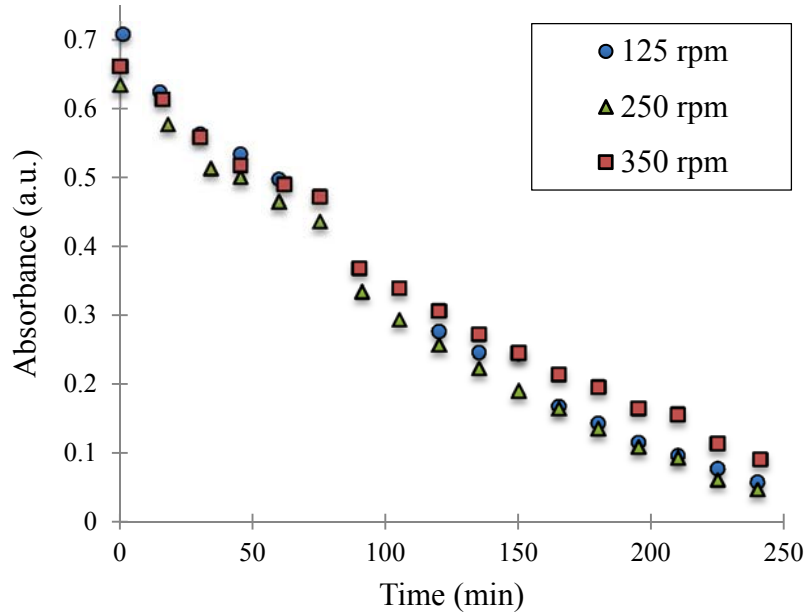


Figure C-4 Effect of Mixing Rate on Methyl Orange Degradation. Study performed with 5% InVO₄-TiO₂ (P-25).

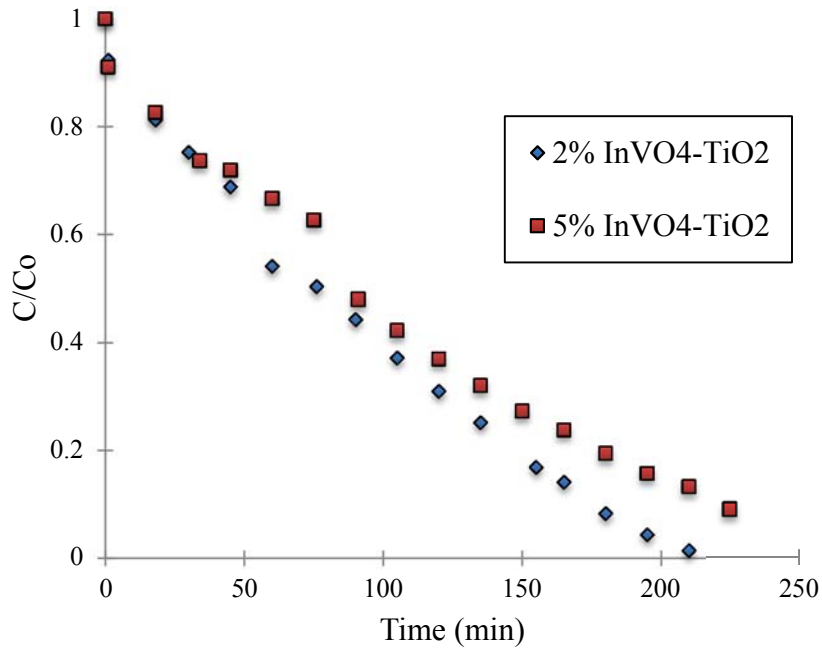


Figure C-5 Effect of InVO₄ Dopant Concentration on Methyl Orange Degradation. Study performed with InVO₄-TiO₂ (P-25) composites.